SCHOOL OF ADVANCED STUDIES OF THE ROMANIAN ACADEMY

DOCTORAL SCHOOL OF CHEMICAL SCIENCES
PETRU PONI INSTITUTE OF MACROMOLECULAR CHEMISTRY

CHEMISTRY Field

POROUS NANOMATERIALS. PREPARATION, PROPERTIES, APPLICATIONS

PhD THESIS SUMMARY

PhD supervisor:
Dr. eng. VALERIA HARABAGIU

PhD student:
MAHU ELVIRA (TURCU)

Iași
2024

Acknowledgements

Upon the completion of this work, I wish to express my deep gratitude and profound respect to all the remarkable individuals who have guided me throughout my research journey.

I extend my most sincere thanks to **Dr. eng. Valeria Harabagiu**, my scientific supervisor, for her meticulous and thoughtful guidance, as well as for the generosity with which she shared her vast professional knowledge. I deeply appreciate her constant support and unwavering encouragement, manifested through her patience and tireless availability, which were essential for the execution and completion of this work. Her professionalism and dedication have been a solid pillar in my academic journey, for which I am profoundly grateful.

I also wish to express my gratitude to **Dr. Maria Ignat**, for her essential contribution to the realization of this doctoral thesis. My deep appreciation goes to her for the ingenious ideas and innovative solutions she provided, as well as for her promptness in responding to my queries. I want to thank her for the trust she placed in my development, for the generous and constant support offered during the challenging moments throughout the thesis development and completion process.

I would like to extend my sincere thanks to my colleagues, **Dr. Petrișor Samoilă** and **Dr. Corneliu Cojocaru**, for their understanding and trust, as well as for their useful advice and constant optimism throughout these years. My deep appreciation goes to them for their unconditional support and their essential contribution to the success of this work.

I also wish to thank the Romanian Academy and the “Petru Poni” Institute of Macromolecular Chemistry for the opportunity to conduct my doctoral research and for providing access to essential infrastructure. I also thank my **colleagues** and **friends** in the institute's departments for their significant contributions to the analyses carried out.

This work was made possible with the financial support of the following research projects: "InnMESO-nonSi" PN-III-P1-1.1-TE-2016-0805, "4WASTEUPGRADE" MySMIS 120696, "INStrEnStD" PN-III-P1-1.1-TE-2021-0762, and "ROFCC" PN-III-P1-1.2-PCCDI-2017-0194.

My deepest appreciation goes to each **member of the doctoral committee** for their time and effort in rigorously and constructively evaluating this work, thereby contributing to its scientific quality and rigor.

Finally, I express my profound gratitude to my family for their unconditional love and invaluable support.

With great consideration,
Mahu Elvira (Turcu)

CONTENTS

LIST OF ABBREVIATIONS AND SYMBOLS.....4

INTRODUCTION.....10

CHAPTER 1. POROUS NANOMATERIALS.....13

1.1 Brief history: from emergence to present.....13

1.1.1 Definition of nanomaterials.....14

1.1.2 Clasification of nanomaterials.....15

1.2 Types of porous nanomaterials.....21

1.2.1 Microporous materials.....23

1.2.2 Mesoporous materials.....24

1.2.3 Macroporous materials.....26

1.1 Methods for the synthesis of porous nanomaterials.....27

1.1.1 Reduction of metal salts.....30

1.1.2 Thermolysis of metal derivatives.....31

1.1.3 Sol-gel synthesis method..... 31

1.1.4 Synthesis in quantum confinement spaces.....34

1.2 Textural properties of porous nanomaterials..... 40

1.3 Areas of interest in the application of porous nanomaterials.....43

1.3.1 Porous materials in environmental applications.....45

CONCLUSIONS.....60

AIMS AND OBJECTIVES.....61

CHAPTER 2. EXPERIMENTAL PART.....64

2.1 Materials used.....64

2.2. Preparations methods.....66

2.2.1. Obtaining titania oxide nanomaterials.....66

2.2.2. Obtaining Co and Ni spinel ferrites.....82

2.2.3. Obtaining porous carbon materials from lignocellulosic biomass.....83

CHAPTER 3. TITANIA OXIDE NANOMATERIALS.....85

3.1 Introduction.....85

3.2 Impact of synthesis parameter variation on TiO_2 nanomaterial preparation.....87

3.3 Study of the effect of ultrasonication regime on TiO_2 characteristics.....95

3.4 Evaluation of the impact of titanium source on TiO_2 properties.....106

3.5 Investigation of the features of TiO_2 nanomaterials generated in the presence of different surfactants.....116

3.6 Trapping experiments of active species.....124

3.7 Optimization of mesoporous titanium oxide synthesis considering surfactant/titanium source ratio and sonication time as control factors.....126

CONCLUSIONS.....135

CHAPTER 4. COBALT AND NICKEL FERRITES WITH SPINEL STRUCTURE....138

4.1 Introduction.....138

4.2 Synthesis of spinel-structured Co and Ni ferrites by microwave-assisted sol-gel combustion method.....139

4.3 Characterization.....142

4.4 Aplications.....150

CONCLUSIONS.....156

CHAPTER 5. CARBON MATERIALS.....158

5.1 Introduction.....158

5.2 Synthesis of carbon materials from lignocellulosic biomass.....160

5.3 Characterization.....161

5.4 Aplications.....181

CONCLUSIONS.....185

CHAPTER 6. GENERAL CONCLUSIONS.....187

PERSPECTIVES.....189

Bibliography.....190

Annex 1. Nanomaterials characterization methods.....220

1 Physico-chemical methods for characterizing prepared titanium oxide nanomaterials.....221

2 Physico-chemical methods for characterizing spinel-structured Co and Ni ferrites.....231

3 Physico-chemical methods for characterizing obtained carbon materials.....233

Annex 2. Scientific activity.....237

Annex 3. Published scientific articles.....242

INTRODUCTION

Nanotechnology is a fascinating field with a highly significant impact on revolutionizing science across various disciplines, such as chemistry, physics, engineering, and biology. It allows for the manipulation of matter at the atomic or molecular level by involving diverse scientific branches, offering unique opportunities for technological development and innovation in multiple areas. In the 21st century, nanoscience and nanotechnology play a crucial role in the industrial revolution, thus nanotechnology is seen as a new driving force for economic growth.

In recent years, the number of products and applications that contain or use nanomaterials has increased considerably. Thus, it is evident that nanotechnology, being a major part of materials science, is also becoming a part of society through the commercialization of nanomaterials. These, through revolutionary changes in shapes, properties, and functions, promote the development of industries such as medicine, agriculture, the environment, aerospace, information sciences, and more, contributing to the improvement of human quality of life [1,2].

The topic of the doctoral thesis holds interest both nationally and at the european level. The doctoral dissertation titled "*Porous Nanomaterials. Preparation, Properties, Applications*" is based on the development of porous nanomaterials such as mesoporous titanium oxide, mesoporous carbon, and Co and Ni ferrites with spinel structure for various applications in photocatalysis and adsorption processes. The first part of the thesis, encompassing **Chapter 1**, reviews the information from the literature on porous nanomaterials, their specific properties, characteristic synthesis methods, and their application areas. In the second part, new synthesis experiments were proposed, developed, and conducted with the aim of improving the properties of the targeted materials. Thus, the original part of the thesis begins with defining the aim and objectives. The following paragraph describes the experimental methods used for preparing mesoporous materials (**Chapter 2**) and continues in the subsequent chapters with the description and interpretation of the original results obtained. **Chapter 3** presents a study on titanium oxide nanomaterials obtained using the sol-gel technique, focusing on the influence of synthesis parameters (ultrasound conditions, the nature of titanium sources, and surfactants) on the physicochemical properties and the evaluation of the photocatalytic properties for degrading organic molecules by the resulting mesoporous materials. The preparation of spinel ferrites $CoFe_2O_4$ and $NiFe_2O_4$ by microwave-assisted sol-gel combustion synthesis using different combustion agents, as well as the characterization of these materials along with the evaluation of

their adsorption properties for organic pollutants, are described in **Chapter 4**. **Chapter 5** presents the pyrolysis processes of lignocellulosic biomass leading to the formation of carbon materials, characterization, and investigation of the sorption properties of these materials for oily liquids.

For each chapter, specific conclusions are listed, followed by the general conclusions and bibliographic sources. At the end of the thesis, the annexes include: methods of characterization of the obtained nanomaterials (Annex I), the scientific activity carried out (Annex II), and copies of published works related to the thesis subject (Annex III).

Purpose and Objectives

The purpose of this study is to establish preparation methods for porous materials with controlled structures and properties through synthesis, as well as to identify and define their application areas.

Throughout the doctoral program, I have proposed and achieved the following objectives:

- **Control of synthesis conditions on the structure and properties of mesoporous titanium oxide (TiO_2)**

  The following parameters were correlated with the properties of the synthesized oxide products:

Ultrasonication regime

- Structural and morphological examination: analysis through FTIR spectroscopy, XRD, and SEM to determine how ultrasonication impacts the crystal structure and morphology.
- Evaluation of textural properties: assessment of adsorption-desorption processes of N_2, and correlation with optical properties using UV-DR
- Photocatalytic processes: investigation of photocatalytic degradation of persistent dyes using the synthesized catalysts, including the identification of active species to elucidate the degradation mechanism.

Nature of the titanium source

- Synthesis and analysis: development of mesoporous titanium oxide with different titanium sources, followed by analysis using SEM, XRD, FTIR, UV-DR, and N_2 adsorption-desorption techniques.;

- Identification of optimal characteristics: determination of the best results in terms of textural, qualitative, morphological, and structural characteristics for implementation in photocatalytic systems.

Nature of the structuring agent

- Structural investigation: analysis of the synthesized oxide materials (XRD), focusing on the influence of different surfactants on crystallite size;
- Textural characterization: examination of the textural properties using the N_2 adsorption-desorption method;
- Identification of functional groups: FTIR analysis to identify characteristic groups of mesoporous titanium oxide, and investigation of morphological properties (SEM) and optical properties;
- Photocatalytic testing: conducting photocatalytic tests and identifying active species to determine the possible degradation mechanism.

Optimization study of control factors in titanium oxide synthesis: influence of the titanium source/surfactant ratio and ultrasonication time:

- Synthesis of TiO_2: the synthesis involved varying the titanium source/surfactant ratio and ultrasonication time to investigate their effects on the physicochemical properties of the synthesized materials;
- Characterization: the study included detailed investigation of the morphological, structural, qualitative, textural, and optical characteristics;
- Photocatalytic application: the synthesized materials were tested in photocatalytic processes under UV light irradiation using an internal lamp.

❖ **Application of an innovative method combining sol-gel synthesis and microwave-assisted autocombustion for the production of cobalt and nickel ferrites with spinel structure**

- Synthesis design: development of sol-gel synthesis methods through autocombustion under microwave influence, using various combustion agents to produce ferrites;
- Characterization: the ferrites were analyzed for textural, morphological, structural, magnetic, and optical properties;
- Adsorption applications: testing $CoFe_2O_4$ and $NiFe_2O_4$ ferrites in adsorption applications.

❖ **Production and valorization of carbon materials from renewable resources.**

- Activated carbon synthesis: synthesis of activated carbon through pyrolysis of vegetal sources;
- Characterization: the carbon materials were characterized using various analytical techniques to determine their physicochemical properties and identify potential application areas, particularly in sorptive processes;
- Sorption testing: the activated carbon was tested for its adsorption capabilities with organic compounds.

CHAPTER 3: TITANIUM OXIDE NANOMATERIALS

This chapter presents a laboratory study that introduces an original approach by investigating the effect of various sol-gel synthesis parameters on the physicochemical characteristics of TiO_2 and their corresponding applicability in the field of photocatalysis.

It was observed that varying the synthesis parameters allows for significant control over the properties of the materials. Literature studies have shown that the surfactant/titanium alkoxide ratio, synthesis method, and nature of the titanium alkoxide influence the textural, structural, and morphological characteristics of TiO_2 [118-120].

Among the known methods for synthesizing TiO_2, the sol-gel technique has garnered significant attention from researchers due to its ability to ensure good chemical homogeneity. Additionally, this technique allows for better control over the physicochemical characteristics of nanomaterials, such as surface morphology, specific surface area, crystallite and nanoparticle size, crystallinity, and phase type, even at relatively low temperatures.

3.2. Impact of synthesis parameter variation in the preparation of TiO_2 nanomaterials

The synthesis of titanium oxide nanomaterials was carried out through sol-gel processes (as depicted in **Scheme 3.1**) for three distinct series of samples, each incorporating variations in synthesis parameters. In this context, the effects of ultrasonication regime, titanium source, and surfactant on the properties of TiO_2 were investigated. The ultrasonication regime was applied in a pulsating manner, alternating between ultrasonic irradiation for several seconds (on) and pauses (off). Various titanium alkoxides ($(RO)_4$-Ti) were used as titanium sources, labeled according to the nature of the R radical: ethyl (TiO_2ET), n-propyl (TiO_2PR), isopropyl (TiO_2IPR), and butyl (TiO_2BU). Nonionic block copolymers (Pluronic F127 and F123) and ionic surfactants (CTAB and SDS), known for their surfactant properties, were employed as surfactants.

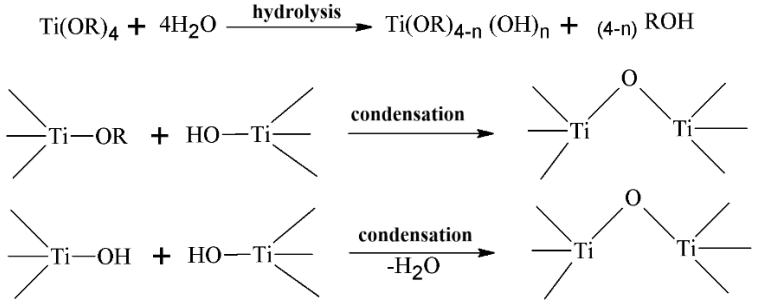

Scheme 3.1. Schematic representation of the hydrolysis and condensation reactions in the synthesis of mesoporous titanium oxide

3.3 Study of the effect of ultrasound regimes on the characteristics of TiO_2

In this study, titanium dioxide (TiO_2) samples synthesized under various ultrasonic regimes were characterized using X-ray diffraction (XRD) to understand the impact of ultrasonic treatment on the crystalline structure of the material. The XRD analysis revealed that the ultrasonic regime significantly influences the nucleation and crystal growth processes, which are crucial in determining the final structure of the TiO_2. The diffractograms displayed characteristic peaks for titanium dioxide at specific 2θ angles, corresponding to the anatase crystalline phase, as identified by the JCPDS 21-1272 standard. These peaks were observed at 2θ angles of 25.4°, 38°, 48°, 54°, 55.2°, 62.8°, 69.14°, 70.18°, and 75.2°. Additionally, the ultrasonic regime can lead to the formation of a secondary brookite phase, indicated by a minor peak at 2θ = 31°.

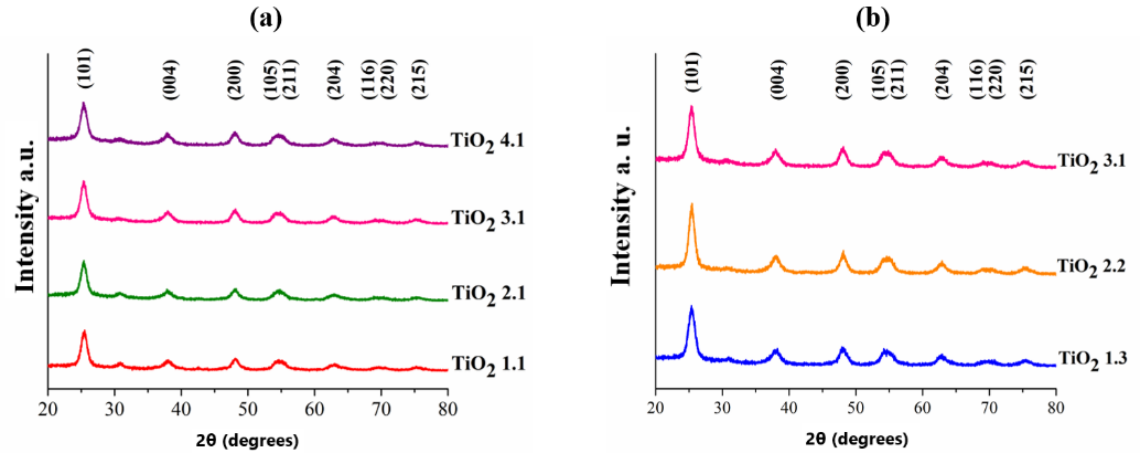

Figure 3.7. X-ray diffraction patterns of samples synthesized under (a) ascending/constant on/off ultrasound regimes and (b) alternating ascending/descending on/off ultrasound regimes

According to the Scherrer equation, the crystallite sizes calculated for the synthesized TiO2 samples ranged between 7.1 and 7.9 nm (as shown in **Table 3.3**). Similar crystallite sizes were also obtained using the Williamson-Hall theory.

Table 3.3. Structural parameters of TiO_2 samples from series I

ID samples	2θ (degrees)	FWHM	$D_{Scherrer}$ (nm)	D_{W-H} (nm)	$d_{(101)}$ (nm)	a_0 (nm)	ε
TiO_2 1.1	25,42	1,15	7,8	8,2	0,35	0,40	0,0047
TiO_2 2.1	25,37	1,18	7,6	7,0	0,35	0,40	0,002
TiO_2 3.1	25,36	1,23	7,3	8,9	0,35	0,40	0,0051
TiO_2 4.1	25,37	1,21	7,4	7,3	0,35	0,40	0,0034
TiO_2 1.3	25,38	1,26	7,1	6,7	0,35	0,40	0,0018
TiO_2 2.2	25,40	1,13	7,9	9,1	0,35	0,40	0,0051

FWHM – Full width at half maximum for the representative peak of anatase (degrees); $D_{Scherrer}$ – crystallite size calculated using the Scherrer equation (nm); D_{W-H} – crystallite size calculated using the Williamson-Hall method (nm); $d_{(101)}$ – interplanar spacing (nm); a_0 – lattice parameter (nm); ε – relative strain.

Considering that a nanomaterial's efficiency in a specific application is significantly influenced by its textural properties, nitrogen sorption measurements were performed to investigate the impact of the applied ultrasound regime during the sol-gel synthesis of TiO_2 on these properties. The six synthesized samples were identified as mesoporous materials with complex pore structures, as classified by IUPAC [148]. The adsorption isotherms obtained were of type IV with H2-type hysteresis loops, characteristic of such materials. Capillary condensation, primarily occurring in mesopores, was observed at relative pressures p/p0 = 0.4-0.8. The type of hysteresis loop varied with the ultrasound regime applied, indicating that adjusting the ultrasound duration can lead to a more uniform pore distribution or the formation of pores within a broader range (3-20 nm).

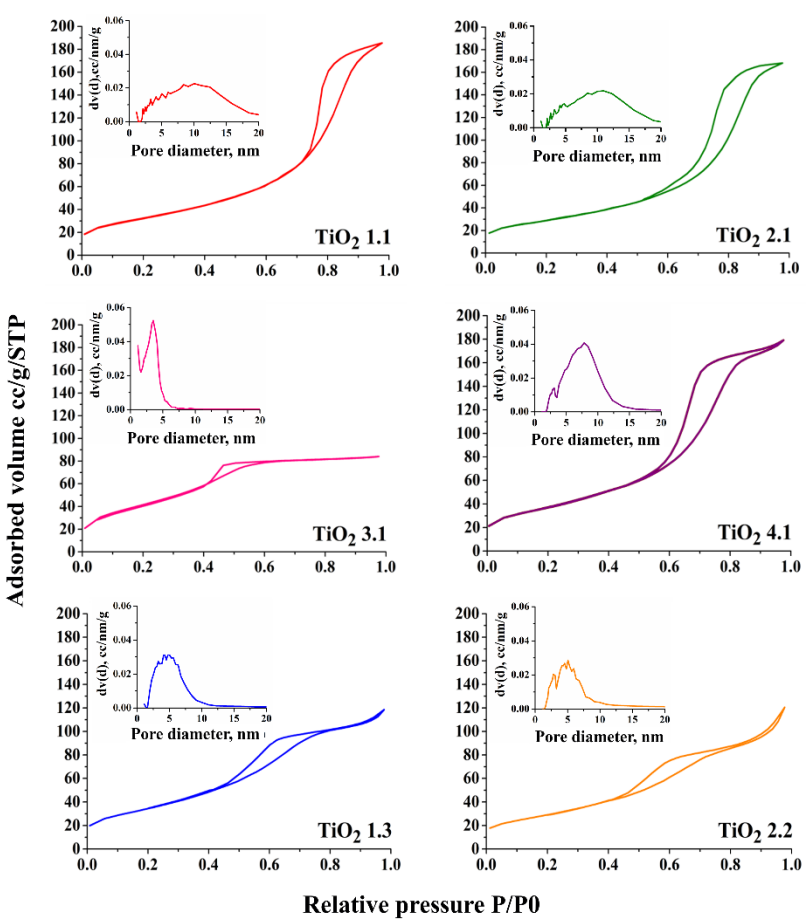

Figure 3.9. Nitrogen adsorption-desorption isotherms and pore size distribution calculated using the BJH method on the adsorption isotherm for the TiO_2 samples from series I

These results suggest that the TiO_2 oxides prepared using the ultrasound-assisted sol-gel technique exhibit optimal properties and characteristics for photocatalytic applications. The samples from series I were tested for the photodegradation of the azo dye Congo Red (CR), which is not susceptible to photolysis under UV light.

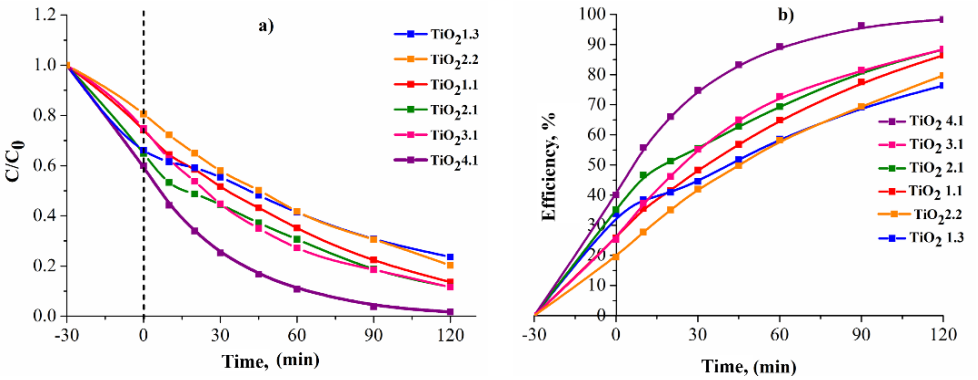

Figure 3.12. **(a)** Adsorption in the absence of light and photocatalytic degradation of CR dye under UV light exposure, **(b)** Efficiency of CR dye removal in the presence of TiO_2 photocatalysts (series I), where the initial pollutant concentration is 50.0 mg/L, catalyst dosage is 1g/L, and temperature is maintained at 20 ± 2 °C.

It was observed that both the amount of dye adsorbed and the degradation rate depend on the nature of the photocatalyst. Before the photocatalytic tests, the CR solution was left in contact with the TiO_2 samples for 30 minutes to achieve adsorption equilibrium. The TiO_2 4.1 sample exhibited the highest adsorption potential (40%). The efficiency of dye degradation increased slightly to values above 70%. **(Figure 3.12)** The best results were recorded for the TiO_2 4-1, $TiO_2$3-1, and $TiO_2$2-1 catalysts, obtained by applying 4on-1off, 3on-1off, and 2on-1off ultrasound regimes, respectively.

3.4 Impact of the titanium source on TiO_2 properties

The study found that the molecular structure and reactivity of different titanium sources used in the sol-gel synthesis of titanium dioxide significantly influence the textural properties of the oxide material, such as porosity, pore size distribution, and specific surface area. Nitrogen adsorption isotherms recorded for the samples in series II **(Figure 3.16)** allowed the evaluation of textural parameters **(Table 3.8)**.

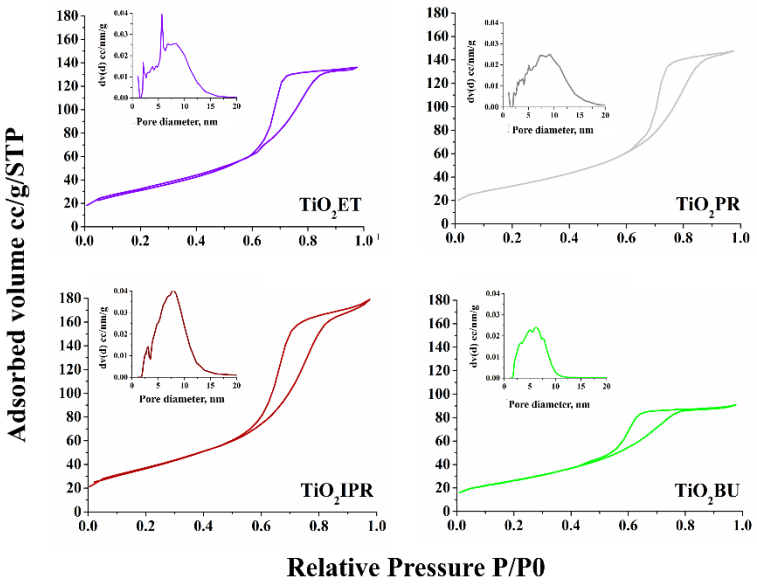

Figura 3.16. Nitrogen adsorption-desorption isotherms and pore size distribution calculated using the BJH method on the adsorption isotherm for the TiO_2 (series II)

Analyzing the data in **Table 3.8**, it is observed that as the number of carbon atoms in the alkyl chain of the titanium source increases, the BET specific surface area of the titanium dioxide decreases. Since the specific surface area values increase similarly to the reactivity of the titanium sources, the samples in series II can be arranged in the order: TiO_2IPR > TiO_2ET > TiO_2PR > TiO_2BU.

Table 3.8. Textural Parameters of TiO_2 Samples (series II)

Sample ID	S_{BET}, m^2/g	V_{tot}, cc/g	D_{por}, nm
TiO_2ET	116	0,20	8,50
TiO_2PR	108	0,22	9,16
TiO_2IPR	136	0,27	7,81
TiO_2BU	98	0,13	5,97

S_{BET} – specific surface BET; V_{tot} – total pore volume; D_{por} – pore diameter.

The effect of the titanium source in the ultrasound-assisted sol-gel synthesis on the morphology of mesoporous TiO_2 was investigated using electron microscopy (SEM and TEM). The study showed that alkoxides with different alkyl chain lengths lead to slightly varied shapes and sizes of titanium dioxide particles, as observed in the images in **Figure 3.17**. These images indicate the aggregation of porous particles, confirming the results of BET analysis.

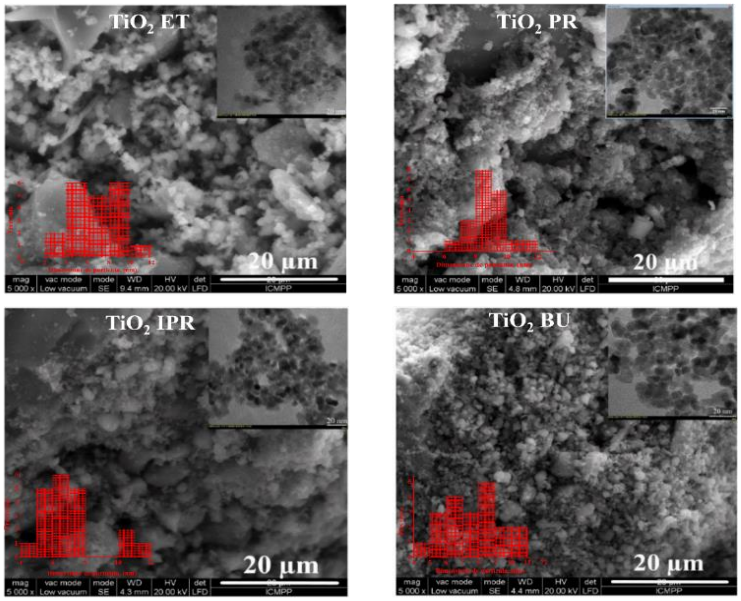

Figure 3.17. SEM and TEM images of the TiO_2 samples synthesized from different titanium sources and histograms representing the particle size distribution (nm)

The titanium oxide materials in series II, synthesized with different titanium sources, demonstrated favorable mesoporous textural and structural characteristics. The TiO_2 sample obtained from titanium isopropoxide exhibited the highest values of specific surface area and pore volume. The crystallite sizes, ordered in decreasing series TiO_2IPR > TiO_2BU > TiO_2PR > TiO_2ET, were predominantly in the anatase phase, sensitive to the UV region. These characteristics recommend these materials as photocatalysts for testing in the photocatalytic degradation of the

CR dye. As seen in **Figure 3.19**, the degradation of CR dye in the presence of the synthesized photocatalysts was successfully achieved.

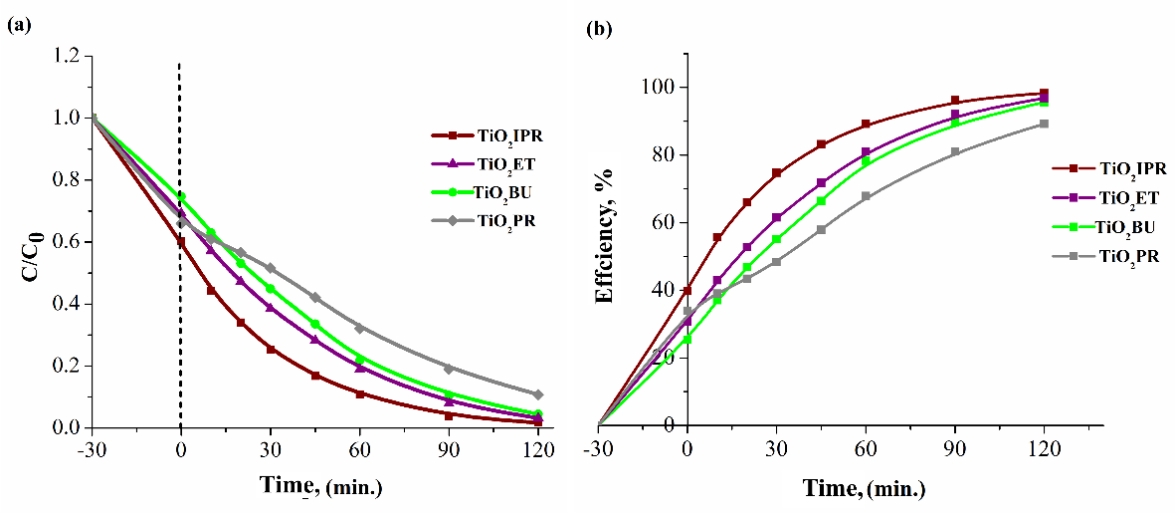

Figure 3.19. Time evolution of dye photodegradation on the surface of TiO_2 catalysts from series II **(a)** and the efficiency of the photocatalysts in CR degradation under UV light **(b)**

3.5 Investigation of the characteristics of TiO_2 nanomaterials generated in the presence of different surfactants

The evaluation of the textural parameters through the nitrogen adsorption-desorption isotherms, represented in **Figure 3.23**, highlights the porous structure, providing insight into how different surfactants used in the synthesis can influence the textural properties of titanium oxide nanomaterials. The isotherms studied for this series (type IV according to IUPAC) indicate mesoporosity with complex pore structures, defined by an H2-type hysteresis

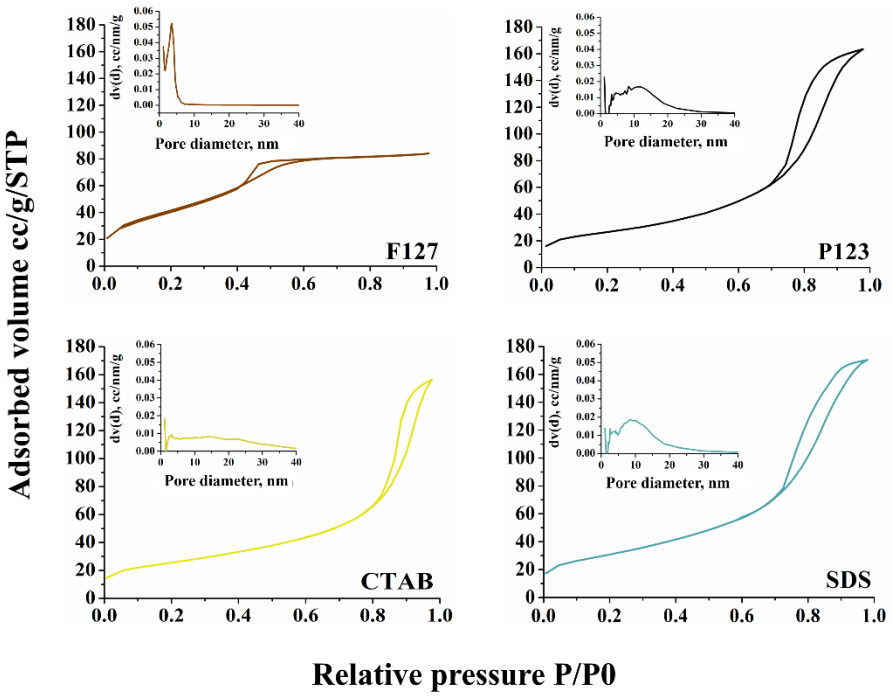

Figure 3.23. Nitrogen adsorption-desorption isotherms and pore size distribution characteristics of TiO_2 samples (series III)

loop. The pore size distributions show that the F127 sample has a narrow and uniform pore distribution, while the other samples exhibit a broader distribution, which can be explained by the different micelle sizes and the interaction between the surfactant and precursor.

The isotherm data were used to calculate specific surface areas (S_{BET}), total pore volumes (V_t), and the average pore diameter (D_{por}) was determined from the pore size distribution graphs **(Table 3.13)**.

Table 3.13 Textural parameters of TiO_2 (series III)

Sample Code	S_{BET}, m^2/g	V_{tot}, cc/g	D_{por}, nm
F127	156	0.13	3.32
P123	88	0,25	10,9
CTAB	87	0,23	3,28
SDS	108	0,26	8,45

Following the analysis of the Tauc plots, the bandgap energy values were determined for each sample. As observed in **Figure 3.25**, the obtained materials exhibit bandgap energy values that are close to those typical for the anatase phase. This indicates that these materials can be activated by UV light, which is advantageous in the degradation processes of hazardous organic substances [163].

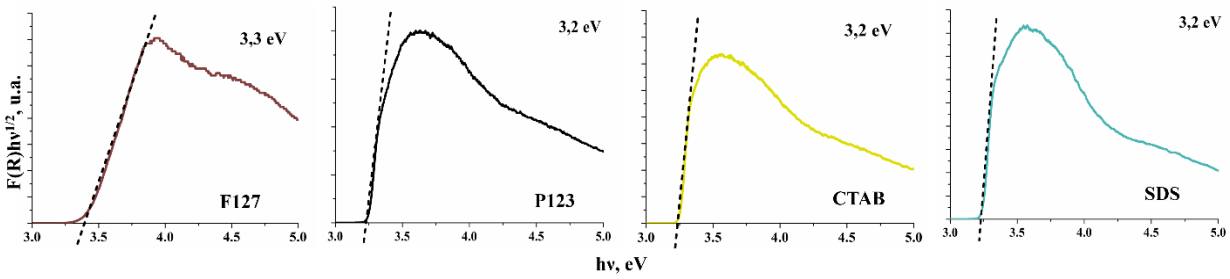

Figure 3.25. Tauc plots of TiO_2 samples (series III)

The materials from series III were tested for their photocatalytic properties in the photodegradation of the CR dye. As shown in **Figures 3.26.a** and **b**, the photocatalytic efficiency decreases in the order of F127 > CTAB > P123 > SDS. The F127 sample exhibits the highest activity in dye degradation, a result that correlates with its textural characteristics, as F127 is the mesoporous material with the highest specific surface area (**Table 3.14**).

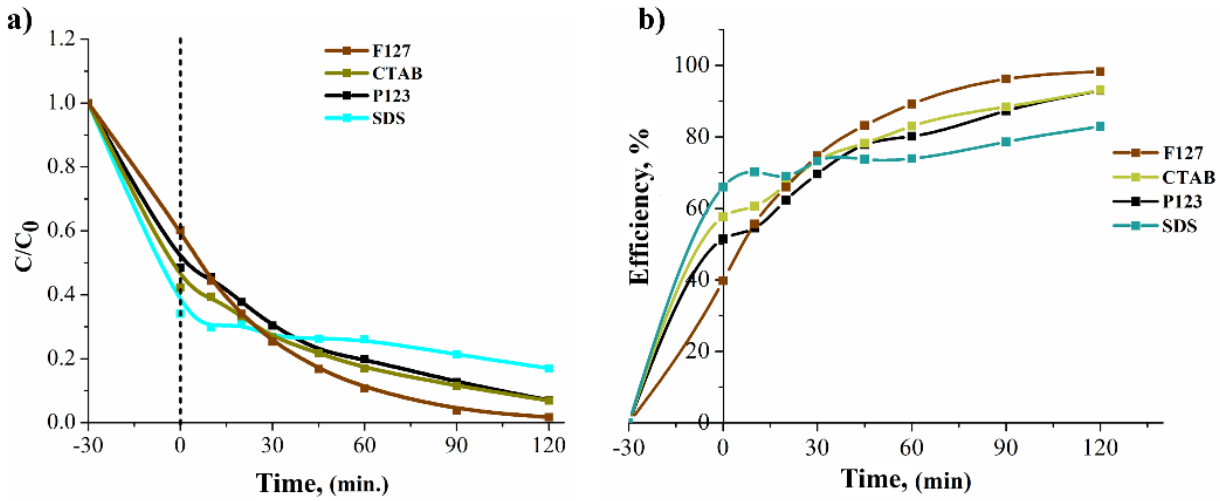

Figure 3.26. Establishing the adsorption/desorption equilibrium of the dye on the catalyst surfaces and the reduction of dye concentration in aqueous solutions during the photodegradation process **(a)** and the efficiency of the catalysts in degrading CR **(b)**

3.6 Trapping experiments of active species

The photocatalytic activity of titanium nanomaterials involves the generation of reactive oxygen species (ROS) when the material is exposed to ultraviolet light. These reactive species, such as hydroxyl radicals (•OH), play a crucial role in the photodegradation of organic contaminants in the environment. In this context, the mechanism of photodegradation of organic molecules in the presence of TiO_2 was investigated. Photodegradation experiments of the CR dye were conducted in the presence of active species scavengers in the reaction medium. Isopropyl alcohol (IPA), hydroquinone (HQ), ethylenediaminetetraacetic acid (EDTA), and potassium chromate (K_2CrO_4) were used as scavengers for hydroxyl radicals HO• [179], superoxide $O_2^{\bullet -}$ [180], holes h^+ [181], and electrons e^-, respectively [182].

The results of these investigations allowed the development of a mechanism for the photodegradation reaction of CR dye on TiO_2 photocatalysts synthesized via the sol-gel method. The schematic representation of this reaction is shown in **Figure 3.29**. By absorbing light energy, the electrons in the valence band (VB) of titanium oxide are excited to the conduction band (CB), leaving positively charged holes in the VB. These photo-generated electrons and holes can either recombine or interact with electron donors or acceptors on the surface of the titanium photocatalyst, such as hydroxyl (-OH) radicals on the surface of TiO_2 or superoxide $O_2^{\bullet -}$ radicals in the reaction medium. These free radicals attack dye molecules and induce oxidation reactions until complete mineralization is achieved [183-185].

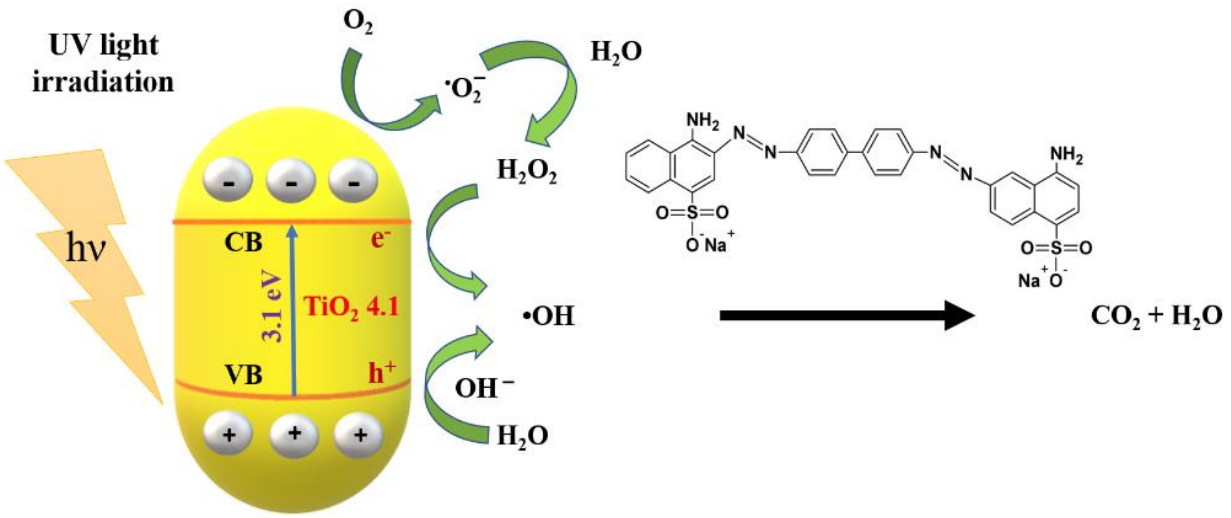

Figure 3.29. Schematic representation of the CR degradation mechanism in the presence of the TiO_2 4.1 photocatalyst

3.7. Optimization of mesoporous titanium oxide synthesis considering surfactant/Ti source ratio and ultrasonication time as control factors.

In addition to varying synthesis parameters, a specific objective of this chapter included an optimization study of control factors in the synthesis of mesoporous titanium oxide. To optimize the synthesis process, a series of nine TiO_2 samples were prepared according to statistical design of experiments (DoE), simultaneously varying the surfactant/Ti source mass ratio and ultrasonication time (**Figure 3.30**).

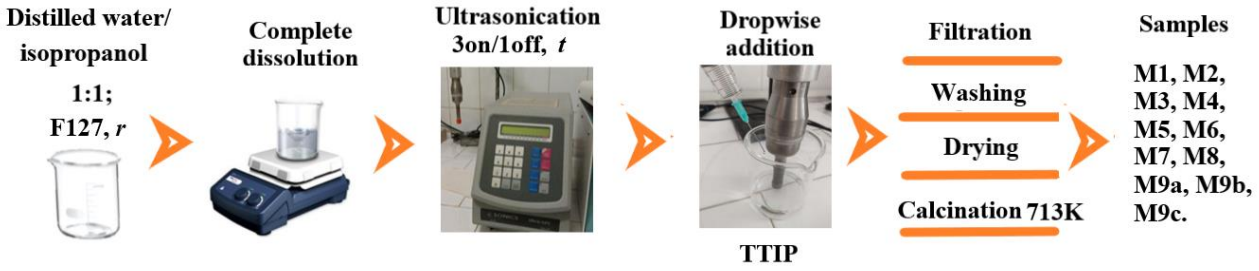

Figure 3.30. Schematic representation of the sol-gel synthesis applied for the preparation of TiO_2 nanomaterials in the optimization study

The study aimed to investigate the factors that can influence the synthesis process and the properties of the resulting materials. Nitrogen adsorption/desorption isotherms were recorded to assess these properties. For each synthesized material in the M1-M9 series, specific surface areas and pore volumes were determined. As seen in **Figure 3.32**, sample M4 exhibits the highest specific surface area of 132 m^2/g and the largest pore volume of 0.331 cm^3/g.

The particle size (histogram in **Figure 3.36**) for sample M5 is D_{TEM} = 8.89 nm, consistent with the crystallite size. Additionally, a selected area electron diffraction (SAED) pattern obtained from TEM (**Figure 3.36**) shows that sample M5 exhibits significant diffraction at low angles, indicating that the titanium oxide material has an ordered porosity.

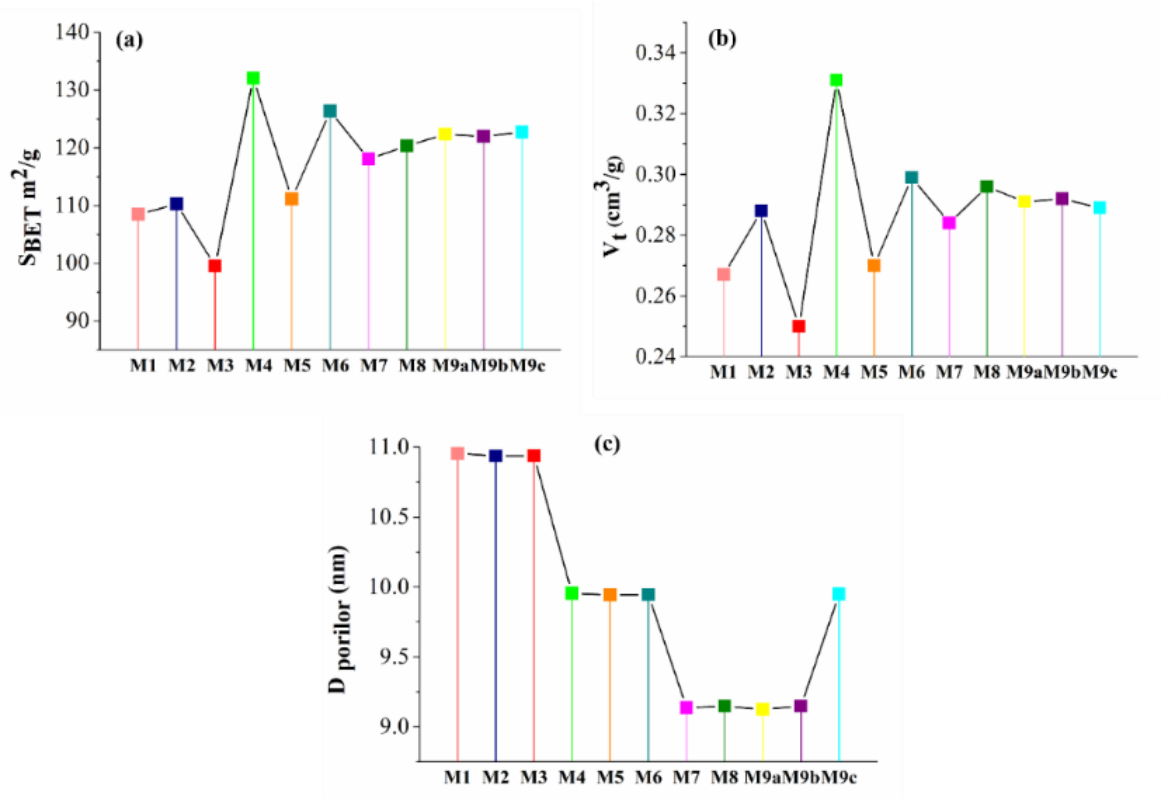

Figure 3.32. Variation of specific surface area (**a**), total pore volume (**b**), and pore size distribution (**c**) for TiO_2 samples

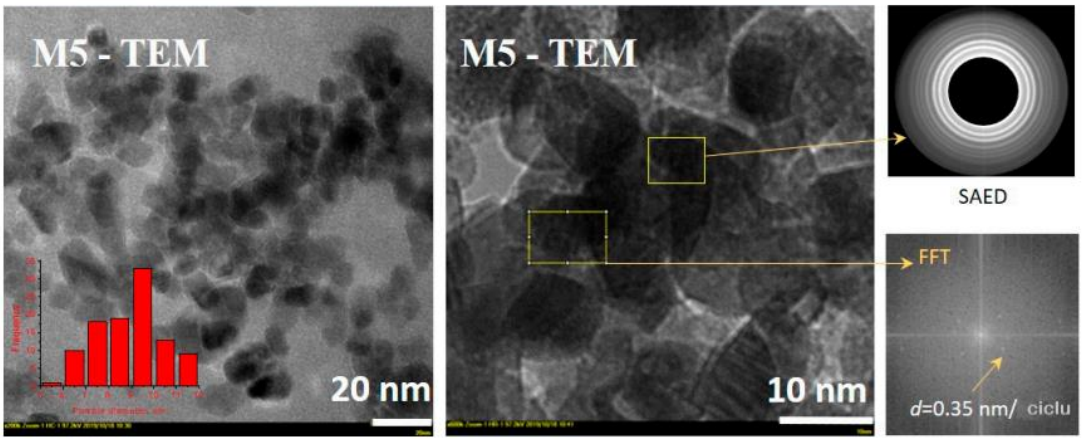

Figure 3.36. TEM images for sample M5 with corresponding particle size distribution histogram and SAED diffraction pattern

The study demonstrated that sample M5, when used in an immersed lamp photoreactor, exhibited remarkable photocatalytic efficiency. **Figure 3.39.a** shows an efficiency of 98.7% in degrading the CR dye within 150 minutes, while the degradation of the 2,4-D herbicide was 50.4% after 240 minutes (**Figure 3.39.b**). This is attributed to the more complex structure of the 2,4-D molecule.

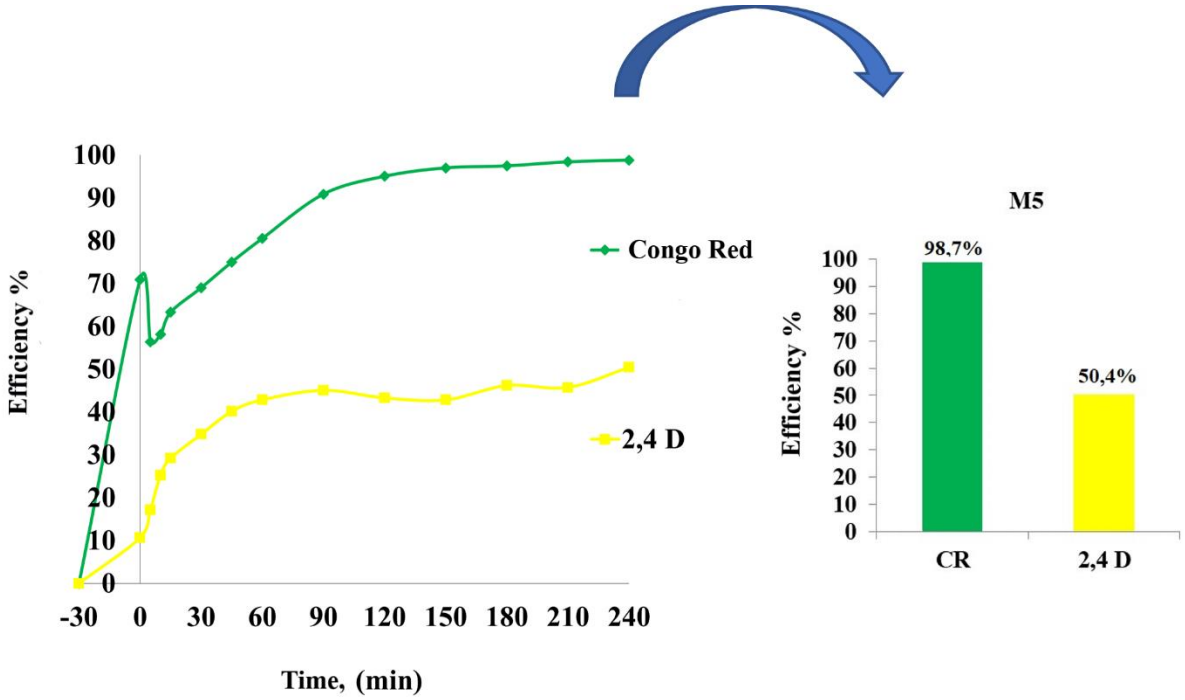

Figura 3.39. (a) Time variation of efficiency in the photodegradation of CR and 2,4-D in the presence of the M5 catalyst, **(b)** Photocatalytic efficiency (%) of sample M5 in degrading CR dye and 2,4-D herbicide

Conclusion

In conclusion, this extensive study initially focused on synthesizing a set of six mesoporous TiO_2 samples using the ultrasound-assisted sol-gel method (series I), with variations in the ultrasound regime. The goal was to identify an optimal ultrasound regime that would promote the formation of materials with suitable physicochemical properties to support superior photocatalytic efficiency. All the obtained materials demonstrated the presence of the anatase phase as the primary phase. As the duration of the "on" cycle in the ultrasound regime increased, a slight reduction in crystallite size was observed (from 7.8 to 7.4 nm). These materials exhibited bandgap energy values (3.1 - 3.2 eV) characteristic of the anatase phase. Considering that a longer ultrasound time in the "on" cycle generated titanium oxide material with a larger specific surface area, this sample (TiO_2 4.1) showed the highest efficiency in degrading the azo dye CR, achieving 98.28% degradation. Consequently, it was found that the titanium oxide nanomaterial obtained under the 4on/1off ultrasound regime showed the highest first-order rate constant in the CR degradation process ($k_1 = 3.0 \times 10^{-2}$ min^{-1}).

A second series of titanium oxide materials was synthesized using different titanium sources. In this case, titanium tetra(isopropoxide) proved to be the source that yielded mesoporous titanium dioxide with the largest specific surface area, 136 m^2/g, and the highest pore volume, 0.27 cc/g. Additionally, the crystallite size was the largest for this sample, with a decreasing trend in the order TiO_2IPR > TiO_2BU > TiO_2PR > TiO_2ET. Corroborated with morphological investigations, the structural results revealed that the particle sizes were the same as the crystallite sizes, presenting a uniform distribution and evident crystallinity, indicating the presence of anatase as the main phase. These improved characteristics of titanium oxide materials, compared to others similarly reported in the literature, recommend them as efficient photocatalysts in the degradation of organic compounds. Thus, the results obtained in the photocatalytic degradation experiments of the CR dye successfully demonstrate the efficiency (over 89%) of the photocatalysts from the series: TiO_2IPR > TiO_2ET > TiO_2BU > TiO_2PR, with the highest photodegradation, 98.28%, achieved by the TiO_2IPR sample.

When another synthesis parameter was modified, namely the type of surfactant (CTAB, F127, P123, SDS) used as a structuring agent in TiO_2 synthesis, a third series of titanium oxide materials was obtained. The results demonstrated that the TiO_2 structure generated by the block copolymer micelles, F127, had the largest specific surface area and the smallest total pore volume.

Additionally, it was observed that the crystallite size differed, following a decreasing trend in the order: CTAB > F127 > P123 > SDS. Once again, anatase was the main phase for which the bandgap energy values were well-known (3.2 eV). However, the photocatalytic efficiency in CR degradation followed a decreasing trend in the order F127 > CTAB > P123 > SDS, with F127 showing an efficiency of 98.2%.

An optimization of the ultrasound-assisted sol-gel synthesis of mesoporous TiO_2 was also carried out, considering two experimental factors as variables. Thus, the ratio between the surfactant and titanium precursor (r), as well as the ultrasound time (t), were varied, applying statistical design (DoE) and response surface methodology (RSM) to identify the optimal synthesis parameters that could lead to the formation of a titanium oxide material with improved photocatalytic activity. The investigations of CR dye and 2,4-D herbicide degradation under UV light revealed that 3 g of Pluronic F127 and 60 minutes of ultrasound were the optimal synthesis parameters for generating a more performant TiO_2 material (sample M5) with maximum degradation efficiencies of 98.4% for CR and 46.3% for 2,4-D. The kinetics of the photodegradation processes followed the pseudo-first-order reaction model, with rate constants of $k_1 = 8.86 \times 10^{-2}$ (min^{-1}) and $k_2 = 6.84 \times 10^{-2}$ (min^{-1}) associated with the (TiO_2 + CR) and (TiO_2 + 2,4-D) systems, respectively. In conclusion, the synergy between crystallite size, specific surface area, porosity, particle morphology, and optical properties was successfully demonstrated, showing a direct dependence on the conditions under which the titanium oxide material was obtained.

Chapter 4. COBALT AND NICKEL FERRITES WITH SPINEL STRUCTURE

4.1 Introduction

This study aimed to obtain and characterize spinel-type ferrites with the formulas $CoFe_2O_4$ and $NiFe_2O_4$. The primary objective of this chapter is to investigate the effect of the nature of the combustion agent on the characteristics of spinel-type ferrites obtained through the sol-gel method, with a novel approach involving microwave-assisted combustion. Additionally, to meet the requirements of adsorption processes, the ferrites were tested as adsorbents for the removal of the Orange II dye from synthetic polluted water.

4.2 Synthesis of Co and Ni Spinel Ferrites by Microwave-Assisted Sol-Gel Combustion

For the synthesis of $CoFe_2O_4$ and $NiFe_2O_4$ ferrites, metal nitrates of iron, cobalt, and nickel were used as cationic sources, while citric acid, maleic anhydride, and urea were employed as combustion agents.

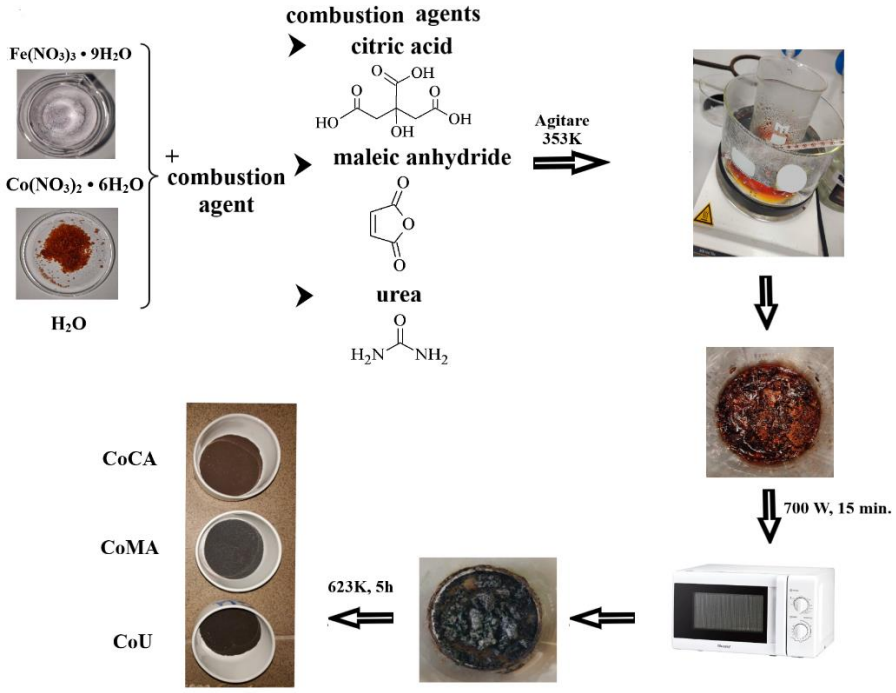

1) $2Fe(NO_3)_3 + Co(NO_3)_2 + 3C_4H_2O_3 + 5O_2 \rightarrow CoFe_2O_4 + 8NO_2\uparrow + 12CO_2\uparrow + + 3H_2O\uparrow$;

2) $2Fe(NO_3)_3 + Co(NO_3)_2 + 3C_6H_8O_7 + 23/2O_2 \rightarrow CoFe_2O_4 + 8NO_2\uparrow + 18CO_2\uparrow + 12H_2O\uparrow$;

3) $2Fe(NO_3)_3 + Co(NO_3)_2 + 3CO(NH_2)_2 + 17/2O_2 \rightarrow CoFe_2O_4 + 14NO_2\uparrow + 3CO_2\uparrow + 6H_2O\uparrow$.

Figure 4.1. Schematic representation of the sol-gel synthesis via microwave-induced combustion of Co ferrite, including the reactions corresponding to each combustion agent: (1) maleic anhydride, (2) citric acid, and (3) urea.

The first step involved dissolving the nitrate species in stoichiometric amounts with the corresponding combustion agent. The mixture was then stirred in a water bath at 80°C until the gel formed. Combustion was triggered by microwave irradiation, after which the obtained materials were subjected to calcination (**Figure 4.1**).

4.3 Characterization

The choice of combustion agent and the use of microwaves significantly affect the textural characteristics of the nanoparticles, as illustrated by the N_2 adsorption-desorption isotherms in **Figure 4.5a,b**. The isotherms for cobalt ferrites (CoMA, CoCA, CoU) and nickel ferrites (NiMA, NiCA, NiU) exhibit a sigmoidal shape characteristic of Type II isotherms, indicating non-porous or macroporous materials. However, the isotherms for NiCA, NiU, and CoU suggest a transition towards Type IV, typical of mesoporous materials, with H3-type hysteresis, indicating slit-shaped pores.

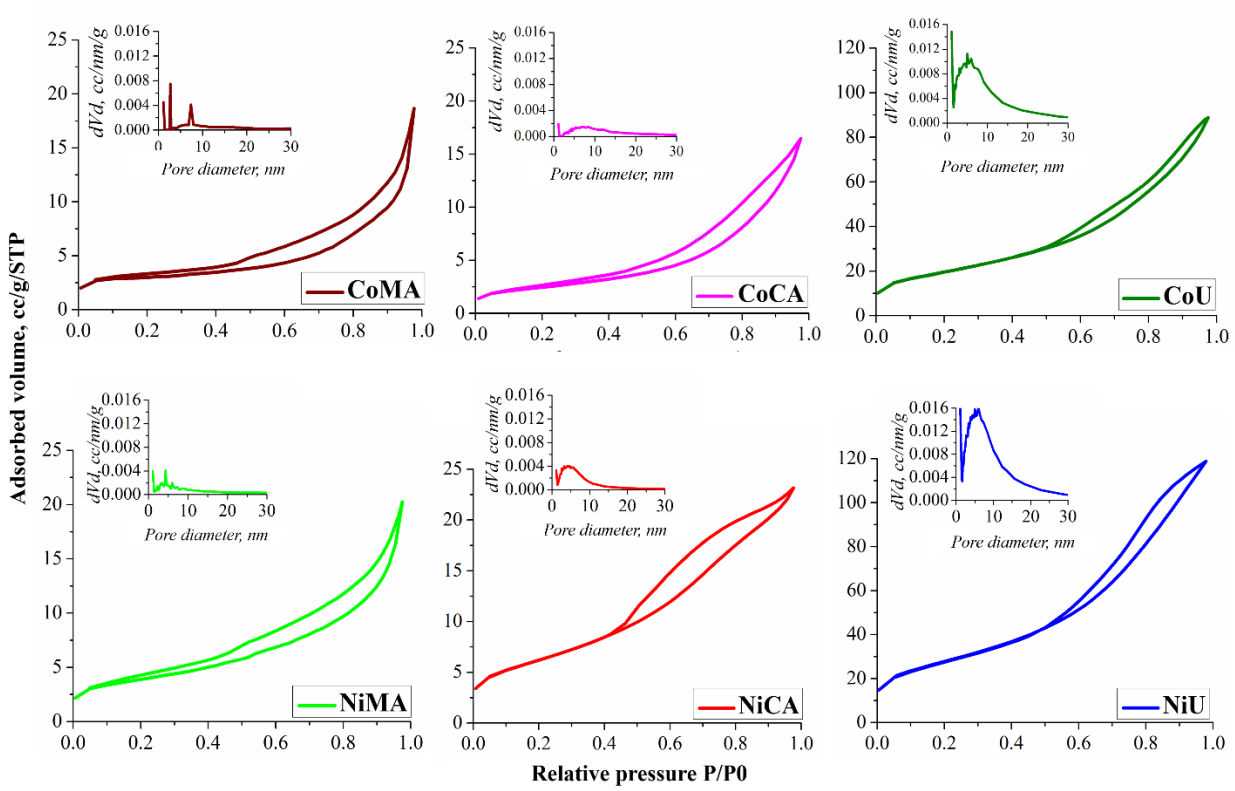

Figure 4.5. N_2 adsorption-desorption isotherms and pore size distribution corresponding to Co and Ni ferrites

The BJH method confirms the mesoporosity of the synthesized materials. The spinel ferrites obtained using citric acid and urea exhibit a broader pore size distribution compared to those synthesized with maleic anhydride (CoAM, NiAM). Specifically, the CoAM and CoAC ferrites have larger pores than CoU, NiAC, and NiU. Table 4.2 presents the specific surface areas (SBET), total pore volumes (Vt), and pore sizes (Dpor) of the studied materials. The nature of the combustion agent significantly influences the specific surface area and total pore volume of the ferrites.

Tabel 4.2. Textural parameters of the synthesized ferrites.

Sample	S_{BET} (m^2/g)	V_t (cm^3/g)	$D_{por.}$(nm)
CoMA	8,3	0,020	2,6; 7,3
CoCA	8,5	0,022	7,2; 12,3
CoU	66,3	0,128	5,03
NiMA	22,0	0,034	3,5; 4,3; 6,0
NiCA	12,6	0,025	4,3
NiU	94,0	0,176	5,9

Combustion agents can induce variations in the microstructure of the material, influencing factors such as crystallite size, grain distribution, and defect density, which in turn affect the magnetic behavior. The magnetic properties of cobalt and nickel ferrites, measured using a Vibrating Sample Magnetometer (VSM) at room temperature, are presented in **Figure 4.8a,b**. Key magnetic parameters, including saturation magnetization and coercivity, are detailed in **Table 4.3**.

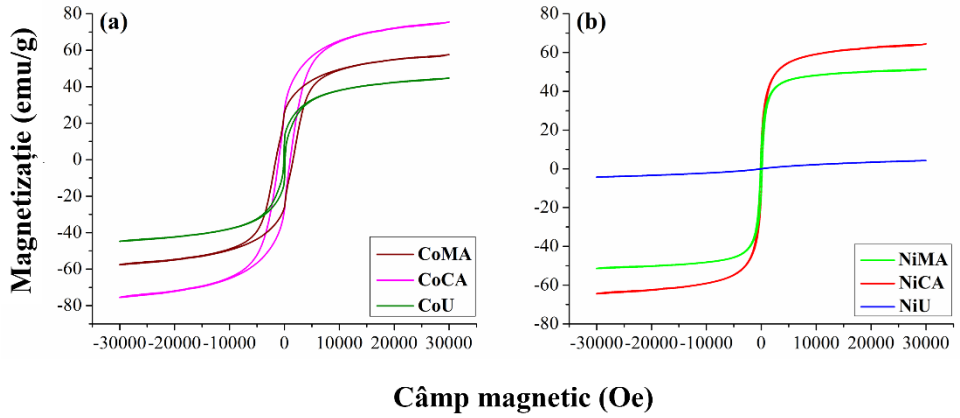

Figure 4.8. Magnetic measurements performed at room temperature for Co (a) and Ni (b) ferrites synthesized via the sol-gel autocombustion method assisted by microwaves using different combustion agents

The results demonstrate a ferrimagnetic [221] behavior for all cobalt and nickel ferrite samples prepared with citric acid and maleic anhydride, and a paramagnetic behavior for the NiU sample [222]. The magnetic properties are correlated with the crystallite size and internal strain. Saturation magnetization decreases as internal strain increases, due to a non-magnetic layer on the surface of the nanoparticles [223].

Tabel 4.3. Magnetic properties of Co and Ni nanoparticles

Sample	Ms (emu/g)	H_c (Oe)
CoMA	76,6	8,0
CoCA	57,4	3,9
CoU	45,4	2,6
NiMA	64,2	3,5
NiCA	51,3	4,2
NiU	4,3	4×10^{-4}

4.4 Applications

The synthesized ferrites were tested for their adsorption capacity of the Orange-II dye from aqueous solutions. The NiU sample ($NiFe_2O_4$) demonstrated the best performance due to its high specific surface area and total pore volume. These properties led to the highest adsorption capacity and efficiency in dye removal, making the NiU sample ideal for kinetic and thermodynamic studies of the adsorption process. The test results are presented in **Figure 4.9**.

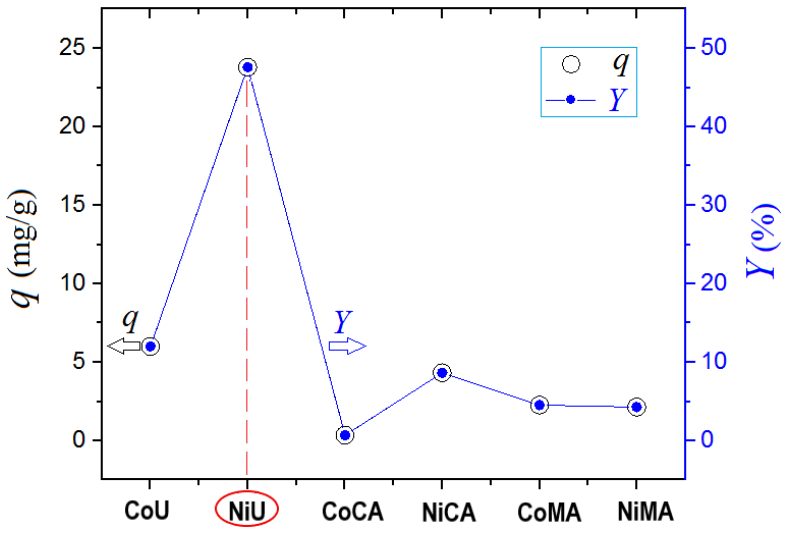

Figure 4.9. Preliminary test for the comparative evaluation of different adsorbents (Co and Ni spinel ferrites) for the removal of Orange-II dye from aqueous solutions: adsorption capacity values (q, mg/g) and color removal efficiency (Y, %) as a function of the adsorbent used.

Kinetics and Adsorption Isotherms

The kinetics of the adsorption of the anionic dye Orange-II on the NiU material was studied at 27 °C, pH 5.0 ± 0.2, with an adsorbent dose of 1 g/L and an initial dye concentration of 50 mg/L. Figure 4.10a shows the variation in adsorption capacity q_t (mg/g) as a function of contact time, t (min). The adsorption capacity increased rapidly in the first 15 minutes, continued to rise gradually between 15 and 120 minutes, and reached an equilibrium plateau after approximately 100 minutes. The experimental data were compared with values obtained by applying various kinetic models, detailed in **Table 4.4**, and expressed through non-linear mathematical equations. The kinetic parameters calculated for each model are also presented in **Table 4.4**.

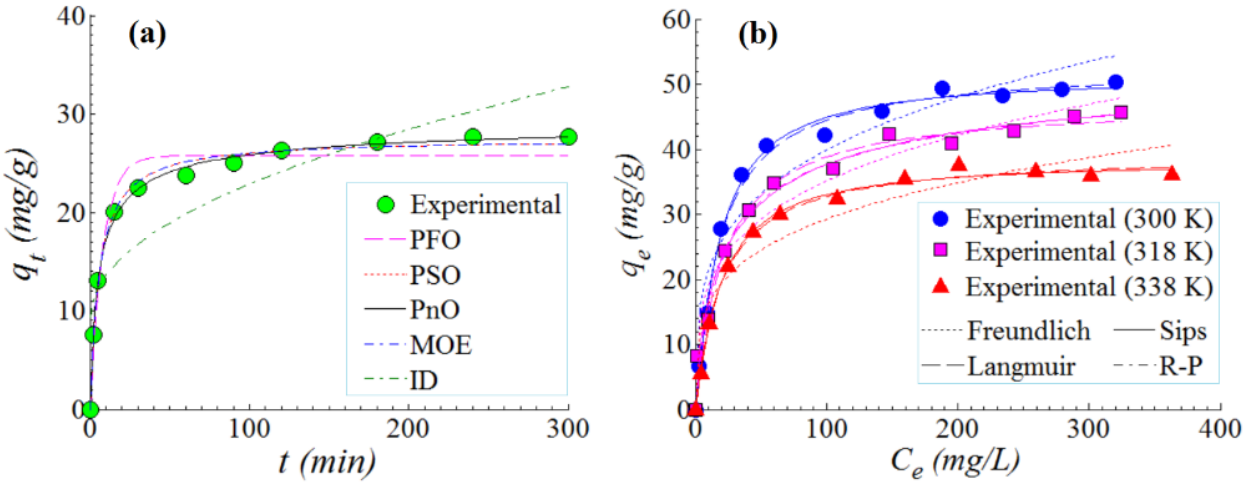

Figure 4.10. Adsorption of the anionic dye Orange-II on the surface of the NiU ($NiFe_2O_4$) adsorbent: (a) adsorption kinetics (data and models) at T=27°CT = 27 °CT=27°C, pH=5.0±0,2pH = 5.0 ± 0,2pH=5.0±0,2, SD=1g/LSD = 1 g/LSD=1g/L, C0=50mg/LC_0 = 50 mg/LC0=50mg/L; (b) adsorption isotherms (data and models), conditions: SD=1g/LSD = 1 g/LSD=1g/L, pH=5.0±0,2pH = 5.0 ± 0,2pH=5.0±0,2, t=360mint = 360 mint=360min; solid, dashed, and dotted lines represent estimates provided by theoretical models.

In **Table 4.4**, q_e (mg/g) and q_t (mg/g) represent the adsorption capacity at equilibrium and at any given time, respectively. The kinetic model parameters were determined through nonlinear regression. The kinetic models are illustrated in Figure 4.10a, and their fit to the experimental data was evaluated using the statistical chi-square test (χ^2). The pseudo-nth order (PnO) model provided the best fit, followed by the mixed-order equation (MOE) and the pseudo-second-order (PSO) model. The PSO rate constant (k_2) for the NiU/Orange-II system was $6{,}36\times10^{-3}$ (g/mg·min^{-1}), which is consistent with values reported in the literature. Adsorption isotherms for the NiU/Orange-II system were recorded at 27, 45 și 65 °C (**Figure 4.10b**), with a contact time of 240 minutes to reach equilibrium. The adsorption capacity q_e (mg/g increased with equilibrium

concentration C_e (mg/L), but decreased with increasing temperature, with the maximum adsorption capacity being 50,32 mg/g at 27 °C.

Tabel 4.4. Kinetic parameters and models for the adsorption of Orange-II dye on the NiU ($NiFe_2O_4$) adsorbent, experimental conditions: T=27°CT= 27 °C: T= 27 °C, SD=1 g/L, $[Orange\text{-}II]_0$ =50 mg/L and pH 5,0 ± 0,2

Model*	Kinetic model (rate equation)	Kinetic model (non-linear equation)	Parameters
PFO	$\frac{dq_t}{dt} = k_1 (q_e - q_t)$	$q_t = q_e \left(1 - e^{-k_1 t}\right)$	q_e = 25.779 (mg/g) k_1 = 1.244 ×10^{-1} χ^2= 1.7115
PSO	$\frac{dq_t}{dt} = k_2 (q_e - q_t)^2$	$q_t = \frac{k_2 q_e^2 t}{1 + k_2 q_e t}$	q_e = 27.501 (mg/g) k_2 = 6.360 ×10^{-3} χ^2=0.2001
PnO	$\frac{dq_t}{dt} = k_n (q_e - q_t)^n$	$q_t = q_e - \left[(n-1) k_n t + q_e^{(1-n)}\right]^{\frac{1}{1-n}}$	q_e = 29.813 (mg/g) k_n = 4.580 ×10^{-4} n = 2.80 χ^2=0.0882
MOE	$\frac{dq_t}{dt} = \sum_i K_i (q_e - q_t)^i$	$q_t = q_e \frac{1 - e^{(-K_1 t)}}{1 - \frac{K_2 q_e}{K_1 + K_2 q_e} e^{(-K_1 t)}}$	q_e = 27.501 (mg/g) K_1 = 2.793 ×10^{-6} K_2 = 6.361 ×10^{-3} χ^2=0.2000
ID	$\frac{dq_t}{dt} = \frac{k_d}{2\sqrt{t}}$	$q_t = k_d \sqrt{t} + J$	k_d = 1.349 J = 9.366 χ^2=7.6391

* PFO – pseudo-first-order model; PSO – pseudo-second-order model; PnO – pseudo-nth order model; MOE – mixed-order equation; ID – intra-particle diffusion kinetic model

The negative value of the Gibbs free energy ΔG (−25,65 kJ/mol) indicates the spontaneous nature of the adsorption process. The negative value of the enthalpy ΔH (−1,46 kJ/mol) suggests a moderate exothermic effect, and the negative entropy ΔS (−75,93 J/mol·K) reflects a reduction in degrees of freedom at the solid/liquid interface. Thus, for the NiU/Orange-II system, all three thermodynamic parameters (ΔG, ΔH, ΔS) are negative, similar to other systems reported in the literature, such as CTAB-modified sepiolite/Orange-II.

Table 4.7. Thermodynamic parameters for the NiU ($NiFe_2O_4$)/Orange-II system

Thermodynamic Parameters		
ΔG (kJ/mol)	**ΔH (kJ/mol)**	**ΔS (J/ mol·K)**
−25,65± 1,46	−1,46	−75,93 ± 0,49

Conclusions

Cobalt ferrite ($CoFe_2O_4$) and nickel ferrite ($NiFe_2O_4$) spinel nanoparticles were successfully synthesized using the sol-gel method combined with microwave-assisted auto-combustion, employing urea, citric acid, and maleic anhydride as combustion agents. The application of microwaves significantly reduced the required time and energy compared to conventional methods. XRD analysis revealed that crystallite sizes and internal strain were influenced by the choice of combustion agent, consistent with BET results. TEM analysis confirmed the irregular shapes and nanometric sizes of the particles. VSM analysis highlighted the ferrimagnetic behavior of the samples, except for the NiU material, which exhibited paramagnetic behavior.

The spinel ferrite materials produced through microwave-assisted sol-gel processing were tested for the adsorption of Orange-II dye from synthetic wastewater, identifying the NiU sample as the most effective. The adsorption kinetics followed the PnO model (n = 2.8), and the Sips isotherm provided the best fit, with a maximum adsorption capacity of 50.32 mg/g at 27°C. According to DR isotherm, the mean free energy ES of sorption ranged from 11.88 to 14.25 ($kJ \cdot mol^{-1}$); suggesting a retention mechanism based on ion-exchange. Along with smaller crystallite size and highest specific surface are, the superiority of NiU sample in adsorption of Orange-II (by ion-exchange predominant mechanism) might be attributed to the paramagnetic behavior of NiU material, compared to other sorbents of ferrimagnetic behavior reported in this study.

CHAPTER 5. CARBON MATERIALS

5.1 Introduction

The main objective of this chapter focuses on the valorization of agricultural waste derived from lignocellulosic biomass through the production of carbon materials. The physicochemical properties of carbon materials, which are crucial for their adsorption capacity, largely depend on the nature of the lignocellulosic source [241,242].

This chapter explores the production of carbon materials from sunflower and corn stalks, which are considered renewable resources. The materials obtained through thermal treatment were thoroughly investigated in terms of their textural, structural, morphological, and surface characteristics (including hydrophilic/hydrophobic properties), which are essential for determining their potential applications. Special attention was given to evaluating the adsorption capacity of these carbon materials as sorbents for oil and petroleum products (such as n-dodecane and 5W-40) from contaminated water.

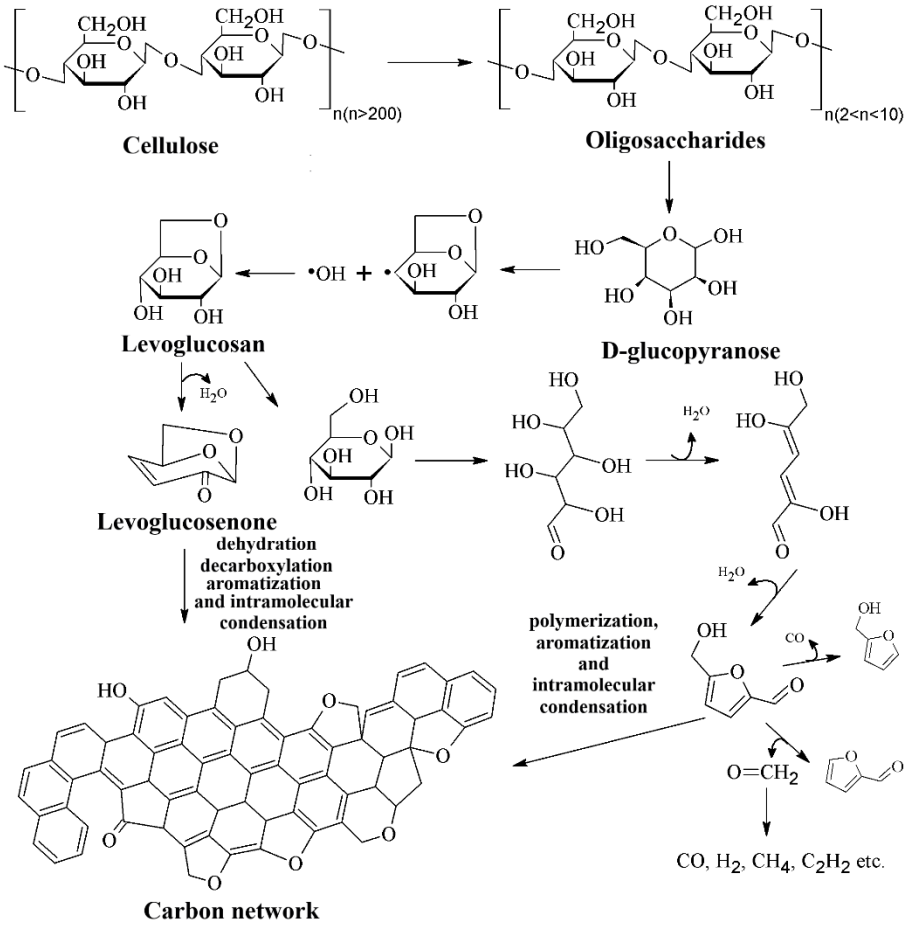

Figura 5.1. Potential mechanism for carbon formation through cellulose pyrolysis [240]

5.2 Synthesis of carbon materials from lignocellulosic biomass

To produce porous carbon materials, two types of agricultural waste were collected: sunflower stalks and corn stalks. The pith from the collected stalks was extracted, dried, and then subjected to pyrolysis in a tubular furnace under a nitrogen (N_2) atmosphere (**Figure 5.2**). The labeling of the vegetal samples and the synthesized carbon materials is presented in **Table 5.1**.

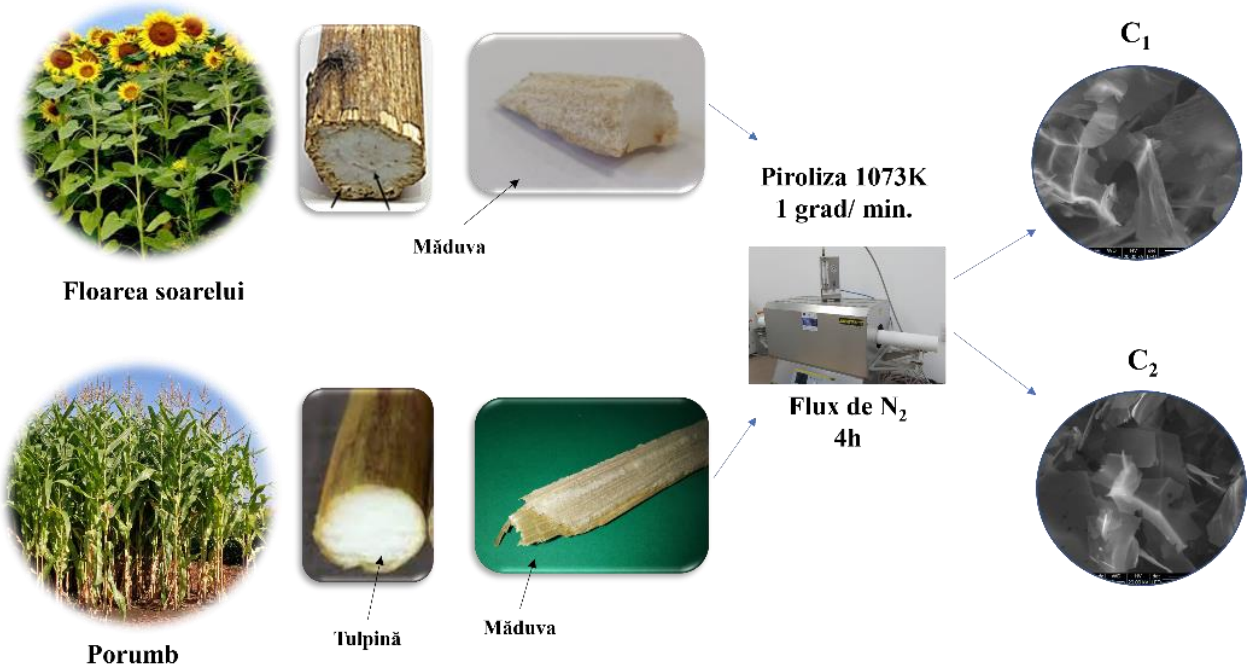

Figure 5.2. Schematic representation of the process for obtaining carbon materials from biomass: sunflower stalk pith and corn stalk pith

Table 5.1. Identification of vegetal samples and synthesized carbon materials

Samples ID	Description
FS	Sunflower stalk (pith), vegetal material.
C_1	Sunflower stalk (pith), carbon material.
P	Corn stalk (pith), vegetal material.
C_2	Corn stalk (pith), carbon material.

5.3 Characterization

The carbon materials obtained were structurally characterized using X-ray diffraction (XRD) (**Figure 5.3**). The diffractograms indicate amorphous structures and varying crystalline domains, with the C1 sample exhibiting more pronounced crystalline domains compared to C2. The higher diffraction peaks suggest a disordered microcrystalline structure, with randomly

oriented graphite microcrystals. Diffraction at high 2θ angles indicates a negligible content of ordered crystalline graphite phase.

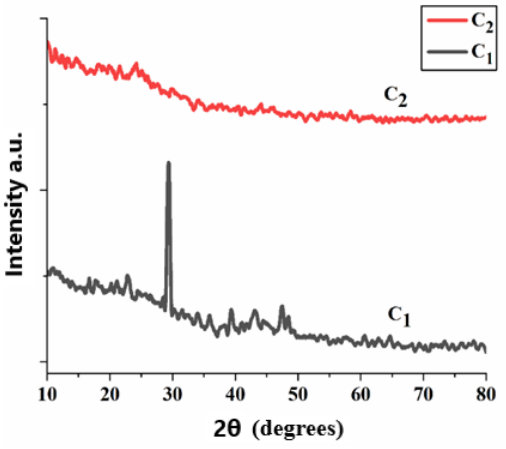

Figure 5.3. X-ray diffraction (XRD) patterns recorded for the carbon material samples, C_1 and C_2

TEM images **(Figure 5.9)** show irregular carbon structures with nanometric porosity. The selected area electron diffraction (SAED) patterns confirm the presence of crystalline domains, indicating the presence of graphite crystallites or other forms of carbon with a lower degree of order.

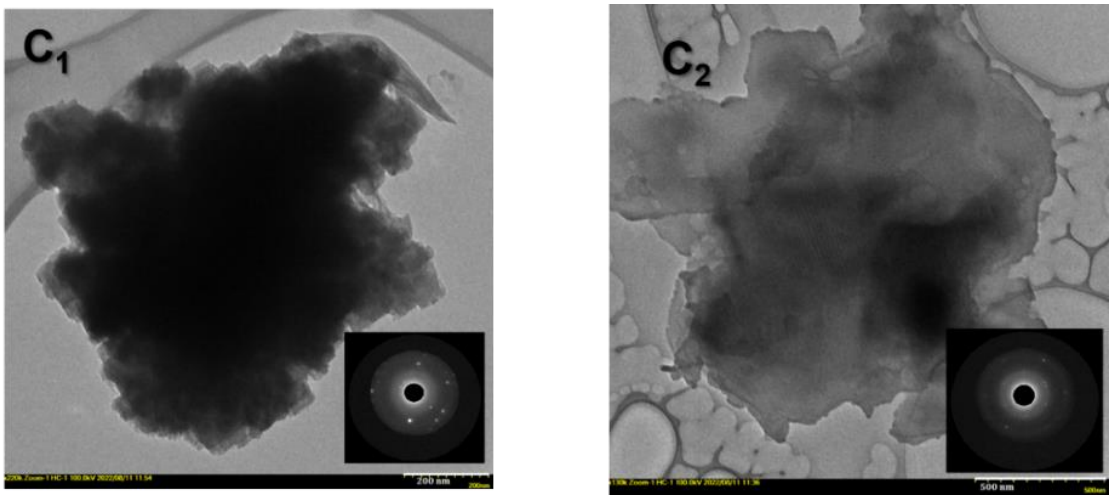

Figure 5.9. TEM images recorded for the C_1 and C_2 samples of advanced carbon materials obtained by conventional methods. SAED images (selected area electron diffraction)

To evaluate the hydrophobic/hydrophilic nature of the carbon materials obtained through pyrolytic synthesis, the contact angles of water droplets on the surface of each material were measured. The recorded images showed angles greater than 90º (**Figure 5.16**), indicating a hydrophobic nature of the carbon surfaces derived from sunflower and corn stalks.

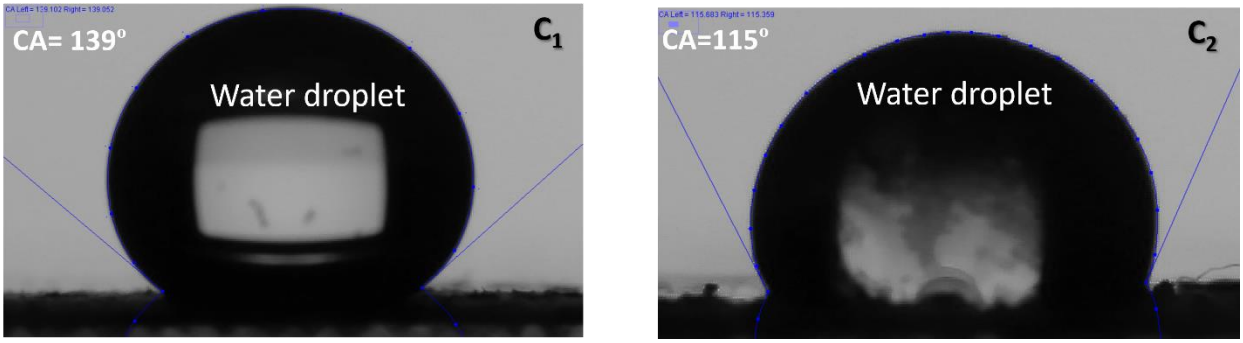

Figure 5.16. Contact angle of water droplets measured on the surface of advanced carbon materials obtained by the conventional method in a tubular furnace

The carbon materials C_1 and C_2, known for their hydrophobic characteristics, were tested for their sorption capacity of petroleum products such as dodecane and motor oil 5W40. The sorption capacity was 9.08 g/g (C1_S) and 9.44 g/g (C2_S) for dodecane, and 9.08 g/g (C1_S) and 5.34 g/g (C2_S) for motor oil. After centrifugation, the retention capacity was 4.09 g/g (C1_Sc) and 4.93 g/g (C2_Sc) for dodecane, and 5.07 g/g (C1_Sc) and 3.39 g/g (C2_Sc) for motor oil **(Figure 5.18)**.

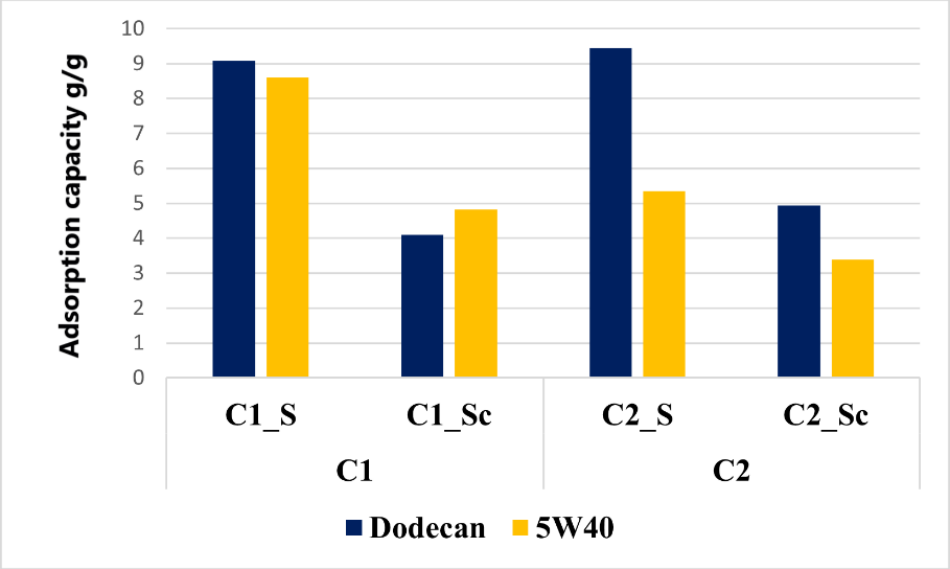

Figura 5.18. Adsorption capacity of oily liquids by the synthesized porous carbon materials.

Conclusions

This study successfully proposed and synthesized carbon materials using abundant lignocellulosic biomass, such as the pith of sunflower and corn stalks. These raw materials were effectively utilized to produce carbon materials with a high carbon content. The investigated samples exhibited varied textural characteristics, with sample C_1 identified as a macroporous solid. Both samples showed amorphous structures with different crystalline domains. FTIR and thermogravimetric analyses highlighted the presence of functional groups associated with cellulose and the complex chemical nature of the materials. The recorded diffractograms revealed a disordered microcrystalline structure, where graphite microcrystals are randomly oriented within the carbon network, and the ordered crystalline graphite phase is nearly negligible. Contact angle measurements indicated the hydrophobic nature of both samples.

The carbon materials demonstrated effectiveness in the sorption of petroleum products, such as n-dodecane and 5W40 motor oil, highlighting their potential as valuable sorbents due to their accessibility and high carbon content. These findings suggest that carbon materials synthesized from lignocellulosic waste can be efficiently used in environmental and industrial applications, thereby contributing to the valorization of renewable resources.

CHAPTER 6. GENERAL CONCLUSIONS

The doctoral thesis is aimed at expanding both theoretical and practical knowledge in the field of porous nanomaterials, focusing on three main categories: (i) titanium oxide nanomaterials; (ii) cobalt and nickel spinel ferrites; (iii) carbon materials.

The first section of the thesis investigates titanium oxide nanomaterials, analyzing the effects of ultrasound regime applied during synthesis. In the first series (series I), it was found that increasing the ultrasound time during the "on" cycle led to higher specific surface areas of the TiO_2 photocatalyst. The titanium sample prepared with a 4on/1off ultrasound regime (TiO_2 4.1) demonstrated optimized physicochemical properties, making it suitable for further photocatalytic applications. Series II highlighted the importance of the titanium source, identifying titanium tetraisopropoxide as the most effective catalyst in the series. The study of surfactants role in TiO_2 synthesis (series III) revealed that the Pluronic F127 surfactant was the most effective, with the F127 sample showing the highest activity in dye degradation, correlated with its textural characteristics. An optimization method was applied to identify the optimal conditions regarding surfactant quantity and ultrasound time. Consequently, the mesoporous titanium oxide obtained under optimal conditions (sample M5) demonstrated maximum efficiencies in removing the azo dye CR and the herbicide 2,4-D.

The oxide catalysts that exhibited maximum photodegradation efficiency (samples from series I, II, and III) were studied to establish a potential mechanism for the photocatalytic degradation of CR dye. The experiments showed that hydroxyl radicals (HO•) are the main reactive oxygen species generated, responsible for the photodegradation process, due to the capture of active species.

The second objective of the thesis focused on cobalt and nickel spinel ferrites, particularly their synthesis through the microwave-assisted sol-gel auto-combustion method using different combustion agents. This study highlighted how the characteristics of spinel ferrites are influenced by the nature of the combustion agent used. A distinctive aspect was the application of microwave energy, which led to the production of spinel ferrites with a significant reduction in time and energy consumption compared to the conventional sol-gel auto-combustion method. The ferrites demonstrated that crystallite sizes and internal strain values are sensitive to the combustion agent used during the synthesis process, consistent with the results of textural characteristics. Furthermore, the ferrites exhibited irregular particle morphology, with sizes in the nanometric range. Regarding magnetic properties, the spinel ferrites showed predominantly ferrimagnetic behavior, except for the Ni ferrite obtained with urea (NiU, $NiFe_2O_4$), which exhibited paramagnetic properties.

The most efficient material for adsorbing the organic pollutant (Orange-II dye) from aqueous solutions was the Ni ferrite sample synthesized with urea. The maximum adsorption capacity was 50.32 mg/g, which was in good agreement with the maximum adsorption capacity predicted by the Sips isotherm

(51.34 mg/g). The DR isotherm suggested an ion exchange-based retention mechanism. To conclude the key aspects related to the efficiency of urea used in Ni ferrite synthesis, it was observed that the smallest crystallite size and the largest specific surface area determined the superior adsorption of Orange-II. This phenomenon can be explained by the paramagnetic properties of the material, in contrast to the ferrimagnetic characteristics of other adsorbents mentioned in this study.

The third objective is defined by the investigation of carbon materials, specifically the synthesis of new carbon materials from the plant biomass of annual plants such as sunflower and corn. The aim of this synthesis was to valorize carbon waste from lignocellulosic biomass, a readily available and economically accessible source. The goal was also to transfer the inherent porosity of the biomass to the resulting carbon material for use in a wide range of applications. The obtained materials are macroporous solids with slit-type pores, featuring amorphous structures and different crystalline domains from one sample to another. The complex nature of the plant samples includes hemicellulose, lignin, and cellulose, and the carbon materials after pyrolysis still present functional groups associated with the cellulose of the plant material. The same observations emerged from the thermogravimetric analysis of these materials, demonstrating the chemical complexity during the thermal process. Each carbon sample shows the presence of graphite crystals or another form of carbon with a lower degree of order. Additionally, strip-like structures/morphologies were observed in the advanced carbon materials obtained, with a carbon content exceeding 60%. The carbon materials exhibit hydrophobic nature and were successfully applied in the sorption processes of petroleum products (n-dodecane and 5W40 motor oil).

PERSPECTIVES

The experience gained during the preparation of the doctoral thesis, as well as the scientific work conducted within the research projects, represents initial achievements in studying the evolution of the investigated porous nanomaterials.

The obtained results will be further explored in the fields of photocatalysis and sorption with the aim of advancing from the conceptual model and laboratory scale to higher production levels.

Bibliography

1. E. A. Bleeker, W. H. de Jong, R. E. Geertsma, M. Groenewold, E. H. Heugens, M. Koers-Jacquemijns, D. van de Meent, J. R. Popma, A. G. Rietveld, S. W. Wijnhoven, F. R. Cassee, A. G. Oomen. *Considerations on the EU definition of a nanomaterial: Science to support policy making.* 1, 2013, Regul. Toxicol. Pharmacol., Vol. 65, pg. 119–125.

2. L. Almeida, I. Felzenszwalb, M. Marques, C. Cruz. *Nanotechnology activities: environmental protection regulatory issues data.* 10, 2020, Heliyon, Vol. 6.

118. T. Benkacem, N. Agoudjil. *Synthesis of Mesoporous Titania with Surfactant and its Characterization.* 11, 2008, American Journal of Applied Sciences, Vol. 5, pg. 1437-1441.

119. D. V. Pinjari, K. Prasad, P. R. Gogate, S. T. Mhaske, A. B. Pandit. *Synthesis of titanium dioxide by ultrasound assisted sol-gel technique: Effect of calcination and sonication time.* 2015, Ultrason. Sonochem., Vol. 23, pg. 185–191.

120. M. Cargnello, T. R. Gordon, C. B. Murray. *Solution-phase synthesis of titanium dioxide nanoparticles and nanocrystals.* 19, 2014, Chem. Rev., Vol. 114, pg. 9319–9345.

147. M. Gharagozlou, S. Naghibi. *Preparation of vitamin B 12 – TiO_2 nanohybrid studied by TEM , FTIR and optical analysis techniques.* 2015, Mater. Sci. Semicond. Process., Vol. 35, pg. 166–173.

148. M. Thommes, K. Kaneko, A. Neimark, J. P. Olivier, F. Rodriguez-Reinoso, J. Rouquerol, K. S. W. Sing. *Physisorption of gases, with special reference to the evaluation of surface area and pore size distribution (IUPAC Technical Report).* 9-10, 2015, Pure Appl. Chem., Vol. 87, pg. 1051–1069.

163. S. Valencia, J. M. Marín, G. Restrepo. *Study of the Bandgap of Synthesized Titanium Dioxide Nanoparticules Using the Sol-Gel Method and a Hydrothermal Treatment.* 2009, The Open Materials Science Journal, Vol. 4, pg. 9-14.

179. C. Coromelci, M. Neamtu, M. Ignat, P. Samoila, M. F. Zaltariov, M. Palamaru. *Ultrasound assisted synthesis of heterostructured $TiO_2/ZnFe_2O_4$ and $TiO_2/ZnFe_{1.98}La_{0.02}O_4$ systems as tunable photocatalysts for efficient organic pollutants removal.* 2021, Ceram. Int.

180. S. Wu, H. Hu, Y. Lin, J. Zhang, Y. H. Hu. *Visible light photocatalytic degradation of tetracycline over TiO2.* September 2019, 2020, Chem. Eng. J., Vol. 382.

181. A. Mancuso, O. Sacco, V. Vaiano, D. Sannino, S. Pragliola, V. Venditto, N. Morante. *Visible light active Fe-Pr co-doped TiO2 for water pollutants degradation.* 2021, Catalysis Today, Vol. 380, pg. 93-104.

182. N. Perciani de Moraes, F. Azooni Torezin, G. Viegas Juca Dantas, J. Giancoli Martins de Sousa, R. Bertholo Valim, R. da Silva Rocha, R. Landers, M. L. Caetano Pinto da Silva, l. Alvares Rodrigues. *TiO_2/Nb_2O_5/carbon xerogel ternary photocatalyst for efficient degradation.* 10, 2020, Ceramics International, Vol. 46, pg. 14505-14515.

183. A. Alshehri, Z. Ahmad Malik, Maqsood Khan, S. A. Al-Thabaitia, N. Hassan. *Biofabrication of Fe nanoparticles in aqueous extract of Hibiscus sabdari ff a with enhanced photocatalytic activities.* 40, 2017, RSC Adv., Vol. 7, pg. 25149–25159.

184. T. Chankhanittha, J. Watcharakitti, S. Nanan. *PVP - assisted synthesis of rod - like ZnO photocatalyst for photodegradation of reactive red (RR141) and Congo red (CR) azo dyes.* 2019, J. Mater. Sci. Mater. Electron., Vol. 30, pg. 17804–17819.

185. B. Bai, L. Qiu, D. Mei, Z. Jin, L. Song, P. Du. *Firmly-supported porous fabric fiber photocatalysts: TiO2/porous carbon fiber cloth composites and their photocatalytic activity*. 2022, Mater. Res. Bull., Vol. 148.

221. K. J. Sankaran, S. Suman, A. Sahaw, U. Balaji, R. Sakthivel. *Improved LPG sensing properties of nickel doped cobalt ferrites derived from metallurgical wastes.* June, 2021, J. Magn. Magn. Mater., Vol. 537.

222. S. Debnath, A. Das, R. Das. *Effect of cobalt doping on structural parameters, cation distribution and magnetic properties of nickel ferrite nanocrystals.* 12, 2021, Ceram. Int., Vol. 47, pg. 16467–16482.

223. V. H. Ojha, K. M. Kant. Investigation of structural and magnetic properties of strained CoFe2O4 nanoparticles. August 2020, 2021, J. Phys. Chem. Solids, Vol. 148.

228. J. Yu, W. He, B. Liu. *Adsorption of acid orange II with two step modified sepiolite: Optimization, adsorption performance, kinetics, thermodynamics and regeneration.* 5, 2020, Int. J. Environ. Res. Public Health, Vol. 17.

240. F. Cheng, X. Li. *Preparation and Application of Biochar-Based Catalysts for Biofuel Production.* 2018, Catalysts, Vol. 1, pg. 1-35.

241. W. Chao, S. Wang, Y. Li, G. Cao, Y. Zhao, X. Sun. *Natural sponge-like wood-derived aerogel for solar-assisted adsorption and recovery of high-viscous crude oil.* May, 200, Chem. Eng. J., Vol. 400.

242. Y. Dai, Z. Jing, Z. Qiu, Y. Zhu, F. Qiu, J. Pan. *Multifunctional biomass carbon fiber aerogel based on resource utilization of agricultural waste-peanut shells for fast and efficient oil – water / emulsion separation.* Mater. Sci. Eng. B, Vol. 283.

Annex 2. Scientific activity

Articles that are the subject of the doctoral thesis:

1. **Mahu, E.,** Ignat, M., Cojocaru, C., Samoila, P., Coromelci, C., Asaftei I., Harabagiu, V. (2020). Development of Porous Titania Structure with Improved Photocatalytic Activity: Response Surface Modeling and Multi-Objective Optimization. ***Nanomaterials***, 10, 988, doi:10.3390/nano10050998. IF: 4,4;
2. **Mahu, E.,** Samoila, P., Ignat, M., Cojocaru, C., Harabagiu, V. (2022). Influence of fuel nature on sol–gel microwave-ignited combustion synthesis of nanosized cobalt and nickel spinel ferrites. ***Comptes Rendus Chimie***, 25 (189-202), 1878-1543. doi: 10.5802/crchim.157. IF:1,6;
3. **Turcu, E.**, Coromelci, C.G., Harabagiu, V., Ignat, M. (2023). Enhancing the Photocatalytic Activity of TiO_2 for the Degradation of Congo Red Dye by Adjusting the Ultrasonication Regime Applied in Its Synthesis Procedure. ***Catalysts***, 13, 345. doi.org/10.3390/ catal13020345. IF: 3,8.

Articles related to the doctoral thesis:

1. Samoila, P., Cojocaru, C., **Mahu, E.**, Ignat, M., Harabagiu, V., (2021). Boosting catalytic wet-peroxide-oxidation performances of cobalt ferrite by doping with lanthanides for organic pollutants degradation. ***Journal of Environmental Chemical Engineering,*** 9, 10496, 2213-3437 doi.org/10.1016/j.jece.2020.104961.
2. **Mahu, E.,** Coromelci, C.-G., Lutic, D., Asaftei, I.-V., Sacarescu, L., Harabagiu, V., Ignat, M. (2021). Tailoring Mesoporous Titania Features by Ultrasound-Assisted Sol-Gel Technique: Effect of Surfactant/Titania Precursor Weight Ratio. ***Nanomaterials***, 11, 1263, . doi.org/10.3390/nano11051263. IF: 5,44

Presentations at national and international conferences:

1 *E. Mahu*, M. Ignat, C. Coromelci-Pastravanu, P. Samoilă, V. Harabagiu, " *Insights into innovative synthesis of mesoporous titania: effect of microwave annealing time on textural and structural properties*", sesiunea de comunicări ştiinţifice a studenţilor, masteranzilor şi doctoranzilor *„*Chimia – frontieră deschisă spre cunoaștere*"*, ediţia a IX-a, 29-30 iunie 2018, Iaşi, România.

2 *E. Mahu*, C. Coromelci-Păstrăvanu, M. Ignat, P. Samoilă, V. Harabagiu, „*Effect of microwave annealing time on nanostructure formation of mesoporous titania photocattalyst*", „XXXV-A Conferința Națională de Chimie", 2-5 octombrie 2018 Călimănești – Căciulata, Vâlcea, România.

3 *E. Mahu*, M. Ignat, C. Cojocaru, P. Samoila, I. Asaftei, V. Harabagiu, „*Development of mesoporous titania with improved photocatalytic activity*", the 12th International Symposium of the Romanian Catalysis Society „RomCat2019", 5-7 iunie 2019, București, România.

4 *E.Mahu*, M. Ignat, C. Cojocaru, P. Samoilă, C. Coromelci-Pastravanu, V. Harabagiu, „*Effect of microwave calcination of mesoporous titania*", Sesiunea de comunicări ştiinţifice a studenţilor, masteranzilor şi doctoranzilor „Chimia – frontieră deschisă spre cunoaștere", ediţia a X-a, 20-21 iunie 2019, Iaşi, România.

5 *E. Mahu*, M. Ignat, C. Cojocaru, P. Samoila, C. Coromelci, V. Harabagiu, "*Correlation of Mesoporous Titania Properties with Titanium Sources Used in the Ultrasound Synthesis Procedure*", the Vth edition of the International Conference „New trends in environmental and materials engineering", 23 – 25 octombrie, 2019, Galați, România.

6 M. Ignat, C. Coromelci, S. Vishkulli, *E. Mahu*, V. Harabagiu, „*A Step Forward in the Development of Titania Photocatalyst Synthesis: Plasma-Induced Porous Structure*", the Vth edition of the International Conference „New trends in environmental and materials engineering", 23 – 25 octombrie, 2019, Galați, România

7 *E. Mahu*, M. Ignat, C. Coromelci, L. Sacarescu, V. Harabagiu, „*Alcoxides as Titania Source: A Study on the Synthesized TiO_2 Properties*", Sesiunea de comunicări științifice a tinerilor cercetători ICMPP – poartă deschisă spre viitor, „MacroYouth'2020", Ediţia I-a, 19 noiembrie 2020, Iaşi, România.

8 M. Ignat, *E. Turcu*, P. Samoila, C. Cojocaru, L. Sacarescu, G. Predeanu, V. Harabagiu, F. Cosmulescu, "*Lightweight carbonaceous materials derived from waste foam-like materials for oil spill remediation*", „14th International Conference on Physics of Advanced Materials", 8-15 septembrie 2022, Dubrovnik, Croația.

9 A.I. Barzic, *E. Turcu*, M. Asandulesa, C. Tugui, R.M. Albu, "*Evaluation of mechanical and dielectric properties of some biodegradable cellulose-based composites*", The 7th International Colloquium „Physics of Materials" – PM 7, 10-11 noiembrie 2022, București, România.

10 *E. Turcu*, M. Ignat, C. Coromelci, L. Sacarescu, V. Harabagiu, " *Study of sunflower and corn stalk pith as raw materials in preparation of carbonaceous adsorbents*", Sesiunea de comunicări științifice a tinerilor cercetători ICMPP – poartă deschisă spre viitor, „MacroYouth'2022", Ediţia III-a, 18 noiembrie 2022, Iaşi, România.

Posters presented at national and international conferences:

1 *E. Mahu*, M. Ignat, P. Samoila, L. Sacarescu, V. Harabagiu, „*Modified sol-gel synthesis of doped TiO2 with rare earth elements*" (Poster P1), the 5th International Conference of the CIS Countries „Sol-Gel Synthesis and Research of Inorganic Compounds, Hybrid Functional Materials and Disperse Systems - «SOL-GEL 2018»", 27-31 August, Sankt-Petersburg, Rusia.

2 *E. Mahu*, C. Coromelci-Pastravanu, M. Ignat, P. Samoila, V. Harabagiu, „*Modified sol-gel synthesis of powdered mesoporous titania: Influence ofmicrowave-annealing on physical properties*", (Poster), „12th International Conference on Physics of Advanced Materials", 22-28 septembrie 2018, Heraklion, Grecia.

3 C. Coromelci, *E. Mahu*, P. Samoilă, C. Cojocaru, M. Ignat, „*Effect of the ultrasound regime used during synthesis on the propersties of mesoporous titania*", (Poster) „XXXV-A Conferința Națională de Chimie", 2-5 octombrie 2018 Călimănești – Căciulata, Vâlcea, România.

4 C. Coromelci, *E. Mahu*, I. Asaftei, D. Lutic, M. Ignat, „*Ultrasound-assisted synthesis of mesoporous titania for efficient adsorbents and photocatalysts obtaining*" (Poster), „IasiChem", 25-26 octombrie 2018, Iași, România.

5 *E. Mahu,* C. Coromelci, D. Lutic, I. Asaftei, M. Ignat, „*Effect of US regime on mesoporous titania properties*", (Poster), „IasiChem", 25-26 octombrie 2018, Iași, România.

6 M. Ignat, C. Coromelci, *E.Mahu* , P. Samoilă, C. Cojocaru, L. Sacarescu, „*One-pot synthesis of porous carbon using surfactant micelles as carbon source in the soft-templated silica synthesis procedure*", (Poster), the 21st Romanian International Conference on „Chemistry and Chemical Engineering", 4-7 septembrie 2019, Constanța, România.

7 *E. Mahu*, M. Ignat, C. Cojocaru, C. Coromelci, P. Samoila, I. Asaftei, V. Harabagiu, „*Comparative study of Congo Red dye and 2,4-diclorophenoxiacetic acid herbicide photodegradation over mesoporous titania*" (Poster), the 21st Romanian International Conference on „Chemistry and Chemical Engineering", 4-7 septembrie 2019, Constanța, România.

8 *E. Mahu*, M. Ignat, C. Cojocaru, P. Samoila, C. Coromelci, V. Harabagiu , „*Photodegradation of congo red dye and 2,4 dichlorophenoxyacetic acid herbicide using mesoporous titania photocatalyst*", (Poster), International Conference ICICH60 "Achievements and perspectives of modern chemistry", 9-11 octombrie 2019, Chișinău, Republica Moldova.

9 *E. Mahu* , M. Ignat, P. Samoila, C. Cojocaru, C. Coromelci, I. Asaftei, V. Harabagiu, „*Influence of titania source on physical properties of mesoporous titania: type of titanium alkoxide*" (Poster), „IasiCHEM", 31 octombrie - 1 noiembrie 2019, Iași, România.

10 *E. Mahu*, M. Ignat, V. Harabagiu, „*Involvement of Various Techniqes in the Synthesis of Titania: Physical Properties Investigations*", (Poster) Sesiunea de comunicări ştiinţifice a studenţilor, masteranzilor şi doctoranzilor, „Chimia – frontieră deschisă spre cunoaștere", ediţia a XI-a, Iaşi, 29-30 Octombrie 2020, România.

Traineeships and mobilities:

"The 3rd Autumn School on Physics of Advanced Materials" (PAMS-3), 22–28 Septembrie 2018, Heraklion, Grecia.

Projects:

1. „Extinderea orizonturilor sintezei inovative a materialelor mezoporoase/structurate ne-silicioase durabile cu funcționalități avansate pentru aplicații de înaltă performanță", cod PN-III-P1-1.1-TE-2016-0805, acronim InnMESO-nonSi, durata: 10.10.2018-30.04.2020.
2. "Motorul revoluţiei energetice bazate pe hidrogen – Pilele de combustibil, pe drumul de la cercetare la producţie prin minimizarea barierelor tehnologice", (ROFCC), Cod proiect: PN-IIIP1-1.2-PCCDI-2017-0194, Contract: 25PCCDI/2018, durata: 09.02.2021-23.04.2021.
3. "Valorificarea inovativă și integrată a deșeurilor biopolimerice prin procese de sinteză inteligente în câmp cu microundecu obținerea de materiale carbonice pentru aplicații de nișă", acronim 4WASTEUPGRADE, cod MySMIS 120696, 12.01.2022-31.01.2023.
4. "Abordări inovatoare de mărire a stocării energiei în dielectrici prin doparea polimerilor verzi cu compuși naturali pentru dispozitive eco-compatibile", acronim INStrEnStD, cod PN-III-P1-1.1-TE-2021-0762, 11.05.2022-01.05.2024.